

Graviton plus vector boson production to NLO in QCD at the LHC

M. C. Kumar^{a,1} Prakash Mathews^{b,2} V. Ravindran^{a,3} Satyajit Seth^{b,4}

^a Regional Centre for Accelerator-based Particle Physics
Harish-Chandra Research Institute, Chhatnag Road, Jhansi,
Allahabad 211 019, India

^b Saha Institute of Nuclear Physics, 1/AF Bidhan Nagar, Kolkata 700 064, India

Abstract

We present the next-to-leading order QCD corrections to the associated production of the vector gauge boson (Z/W^\pm) and the graviton in the large extra dimension model at the LHC. We estimate the impact of the QCD corrections on the total cross sections as well as the differential distributions of the gauge bosons and find that they are significant. We also study the dependence of the cross sections on the arbitrary factorization scale and show the reduction in the scale uncertainties at NLO level. Further, we discuss the ultraviolet sensitivity of the theoretical predictions.

Key words: Large Extra Dimensions, NLO QCD

¹mckumar@hri.res.in

²prakash.mathews@saha.ac.in

³ravindra@hri.res.in

⁴satyajit.seth@saha.ac.in

1 Introduction

The standard model (SM) of particle physics has been very successful in explaining the fundamental interactions of the elementary particles, and its predictions have been verified experimentally to a very good accuracy except for the discovery of the Higgs boson, the only elementary scalar particle in the SM. In spite of its merits, the SM has many open questions that are not addressed within its domain and a plenty of room is left open for some beyond SM physics scenarios to address them. Supersymmetry, extra dimensions, techni-color models are a few to name such beyond SM scenarios. With the advent of the high energetic hadron colliders like Tevatron and the Large Hadron Collider (LHC), it is quite feasible to probe these new scenarios in the laboratory experiments. The LHC with its unprecedented center mass energy of 14 TeV and with luminosities as high as $10^{34} \text{ cm}^{-2} \text{ s}^{-1}$, offers the best possibility of discovering not only the elusive Higgs boson but also of the possible new physics that is hidden so far at lower energies. On the other hand, the Tevatron which is operating at a center of mass energy of 1.96 TeV has been probing such new scenarios.

One of such beyond SM scenarios that have gained a lot of interest and have been studied well in the context of collider phenomenology is the large extra dimensional (LED) model proposed by Arkani-Hamed, Dimopoulos and Dvali [1]. This model is theoretically well motivated and it addresses the hierarchy problem with the concept of extra spatial dimensions. The size of the extra dimensions in this model can be of macroscopic size but still consistent with the data from the experiments to date. A viable mechanism to hide these extra d spatial dimensions from the SM particles is to confine the latter to a 3-brane and allow only the gravity to propagate the full $4 + d$ dimensional space time. For simplicity, the extra dimensions can be assumed to be flat, of the same size and compactified on a d -dimensional torus of radius $R/(2\pi)$. After the compactification, the scale M_s of the extra dimensional theory is related to the Planck scale M_p as:

$$M_p^2 = C_d M_s^{2+d} R^d \quad (1)$$

where $C_d = 2 (4\pi)^{-\frac{d}{2}}/\Gamma(d/2)$ and R is the size of the extra dimensions. This compactification implies that a massless graviton propagating in $4 + d$ dimensions manifests itself as a tower of massive graviton modes in 4-dimensions, with mass $m_{\vec{n}}^2 = 4\pi^2 \vec{n}^2/R^2$ where $\vec{n} = \{n_1, n_2, \dots, n_d\}$ and $n_i = \{0, 1, 2, \dots\}$. Here, the zero mode corresponds to the 4-dimensional massless graviton. As the inverse square law of gravity has been tested down to only few μm so far [2], the size of the extra spatial dimensions in this model can be taken as large as this limit. The hierarchy between the electroweak scale and the Planck scale can then be accounted for by this large volume of the extra dimensions, as can be seen from eqn.(1). For $M_s \sim \mathcal{O}(\text{TeV})$, the above limit on R constrains the number of extra dimensions to $d \geq 2$.

In the effective theory valid below the scale M_s , these gravitons couple to the SM fields through energy momentum tensor $T^{\mu\nu}$ of the latter with the coupling

$\kappa = \sqrt{16\pi}/M_p$, as given by [3, 4]

$$\mathcal{L}_{int} = -\frac{\kappa}{2} \sum_{\vec{n}=0}^{\infty} T^{\mu\nu}(x) h_{\mu\nu}^{(\vec{n})}(x). \quad (2)$$

Since the coupling is through the energy momentum tensor, the gravitons can couple to all the SM fields with the same coupling strength κ irrespective of their charge, color and flavor. The Feynman rules for the above interaction lagrangian are given in [3, 4, 5] and in the first reference of [6]. To order κ^2 , the above action allows processes involving SM fields and virtual gravitons in the intermediate state or real gravitons in the final state. In the context of collider phenomenology, this gives rise to a very rich and interesting signals that can be seen at the LHC. The virtual exchange of the gravitons can lead to the deviations from the SM predictions whereas the real emission of the gravitons can lead to the missing energy signals. Though the coupling of each graviton mode to the SM fields is M_p suppressed, the large multiplicity of the available graviton modes can give rise to observable effects. Hence, there will be a summation over the graviton modes at the amplitude level for the virtual graviton exchanges, and at the cross section level for the real graviton emissions. As the size of the extra dimensions could be large in this model, the mass splitting i.e. $2\pi/R$ is very small and hence this summation over the graviton modes can be approximated to be an integral in the continuum limit, with the density of the graviton modes given by [4]

$$\rho(m_{\vec{n}}) = \frac{R^d m_{\vec{n}}^{d-2}}{(4\pi)^{d/2} \Gamma(d/2)} \quad (3)$$

For the real graviton production process at the collider experiments, the inclusive cross section is given by the following convolution:

$$d\sigma = \int dm_{\vec{n}} \rho(m_{\vec{n}}) m_{\vec{n}}^{d-1} d\sigma_{m_{\vec{n}}} , \quad (4)$$

where $d\sigma_{m_{\vec{n}}}$ is the cross section for the production of a single graviton of mass $m_{\vec{n}}$. This collective contribution of the graviton modes results in their non-negligible interaction with the SM fields, and offers the best possibility of probing the low scale quantum gravity effects at the colliders experiments. Consequently, a very rich and interesting collider signals of some important processes have been reported in the literature, but most of them are available only at the leading order (LO) in the perturbation theory [3, 4, 7, 8, 9]. At the hadron colliders like LHC or Tevatron, the QCD radiative corrections are very significant for they can enhance the LO predictions as well as decrease the arbitrary scale uncertainties in theoretical predictions. Further, the presence of a hard jet in the final state, due to these radiative corrections, has the potential to modify the shapes of the transverse momentum distributions of the particles that are under study at LO. Obtaining such a modification to the shapes of the distributions is beyond the scope of the normalization

of the corresponding LO distributions by a constant K-factor, and it requires an explicit computation of the cross sections or distributions to next-to-leading order (NLO) in QCD. Owing to this importance of the radiative corrections, they have been computed for some important processes involving virtual or real graviton effects. The K-factors in some cases are found to be as high as a factor of two. Pair production processes are the best to exemplify the case of virtual graviton effects, where the NLO QCD corrections are computed for di-lepton [6], di-photon [10], di-Z and $W^+ W^-$ [11] production processes. In the context of missing energy signals in the large extra dimensional model, the NLO QCD corrections are presented for the processes (i) jet plus graviton production [13] and (ii) photon plus graviton production [14]. In each of these two cases, it is shown that the K-factors can be as high as 1.5 at the LHC.

In the present work, we compute the NLO QCD corrections to the associated production of vector gauge boson and the graviton at the LHC and give a quantitative estimate of the impact of these radiative corrections. The paper is organized as follows. In sec.2, we discuss the importance of graviton plus vector gauge boson production process, outline the phase space slicing method for computing the NLO QCD corrections and present the analytical results. In sec.3, we give the numerical results for both the neutral gauge boson and the charged gauge boson cross sections. Finally, we present the conclusions in sec.4.

2 Graviton plus vector boson production

The gravitons when produced at the collider experiments escape the experimental detection due to their small couplings and negligible decays into SM particles. The production of vector bosons ($V = Z, W^\pm$) together with such an *invisible* gravitons (G) can give rise to a very large missing transverse momentum signals at the collider experiments. The study of graviton plus gauge boson production, hence, in general will be a useful one in probing the new physics at the LHC. This process has been studied at leading order (LO) in the context of lepton colliders [15, 16] as well as at the hadron colliders [17], and also has been implemented in Pythia8 [18]. The process is an important one and stands complementary to the more conventional ones involving the graviton production, like jet plus graviton or photon plus graviton productions, that are generally useful in the search of the extra dimensions at collider experiments.

It is important to note that there is a Standard Model (SM) background which gives signals similar to those of associated production of Z and G . This SM background receives a dominant contribution coming from the ZZ production process, where one of the Z -bosons in the final state decays into a pair of neutrinos ($Z \rightarrow \nu\bar{\nu}$) leading to Z -boson plus missing energy signals. The other Z -boson can be identified via its decays to leptons, mostly electrons and muons, and then constraining the lepton invariant mass close to the mass of the Z -boson to consider only the on-shell

Z -bosons. A detailed study of the event selection and the minimization of other SM contributions to this process $ZZ \rightarrow \bar{l}l\nu\bar{\nu}$, using MC@NLO and Pythia, is taken up in the context of ATLAS detector simulation and is presented in [19]. Any deviation from this SM prediction will hint some beyond SM scenario and hence a study of this process will be useful in searching the new physics.

In the context of extra dimensions, a study of the Z plus graviton production at LO at the LHC is discussed in [17], where the Z -boson identification is done with the leptonic decay modes and using the cuts on the leptons as specified in [19]. At the LHC, a similar study is done where the signals of Z -boson plus missing energy in this model are compared against those coming from the SM ($Z\nu\bar{\nu}$) background and are presented in our recent study [20]. It is worth noting here that a signal of Z -boson plus missing energy can also come from the production of Z plus unparticle \mathcal{U} , where the unparticle leads to missing energy signals. A study of such process based on ATLAS detector simulation [17] shows that the vector unparticles are difficult to be probed using this channel, whereas the tensor unparticles can give signals identical to that of the graviton. In view of the above, it is worth studying the Z plus missing energy signals, in particular ZG production, which will be useful to confirm the extra dimensional signals once they are seen in the main channels like jet or photon plus missing energy.

In what follows, we describe the computation of NLO cross sections for the process under study. Since our focus is on the QCD part in this work, we will confine our calculation to the production of on-shell Z -boson. A more detailed study involving the Z -boson decays into leptons requires a full detector level simulation with the appropriate cuts at NLO and is beyond the scope of the present paper.

2.1 Leading Order Calculation

At the lowest order in the perturbation theory, the associated production of the vector gauge boson and the graviton takes place via the quark anti-quark initiated subprocess, given by

$$q_a(p_1) + \bar{q}_b(p_2) \rightarrow V(p_3) + G(p_4), \quad (5)$$

where $V = Z, W^\pm$ and a, b are flavor indices. The corresponding Feynman diagrams are shown in Fig. (1). These diagrams are obtained by considering the tree level $q\bar{q}V$ diagram and by attaching the graviton line to all the possible external legs and the $q\bar{q}V$ vertex. The Feynman rules and the summation of polarization tensor of the graviton are given in [3, 4]. The couplings of the fermions to the Z and W bosons are given by

$$-i\frac{eT_Z}{2}\gamma^\mu(C_v - C_a\gamma^5), \quad -i\frac{eT_W}{2}\gamma^\mu(1 - \gamma^5) \quad (6)$$

where

$$T_Z = \frac{1}{\cos\theta_W \sin\theta_W}, \quad T_W = \frac{1}{\sqrt{2} \sin\theta_W}$$

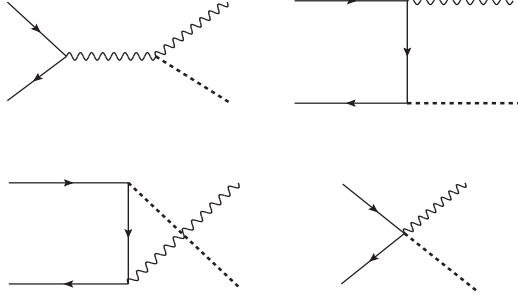


Figure 1: Feynman diagrams that contribute to the associate production of the vector boson and the graviton at the leading order.

and the coefficients C_v and C_a are

$$C_v = T_3^f - 2 \sin^2 \theta_W Q_f, \quad C_a = T_3^f \quad (7)$$

Here, Q_f and T_3^f denote the electric charge and the third component of the isospin of the quarks respectively, and θ_W is the weak mixing angle. For the vector gauge boson, the propagator in the unitary gauge ($\xi \rightarrow \infty$) has been used throughout. This choice of the unitary gauge in the electro weak sector has the advantage of having vanishing goldstone and ghost contributions. The leading order matrix elements for the associated production of Z -boson and the graviton are computed using the algebraic manipulation program FORM [21] and are given by (in n -dimensions)

$$\begin{aligned} \sum_{spin} |\overline{M}|^2 &= \frac{1}{4} \frac{1}{3} \frac{1}{96} (C_v^2 + C_a^2) \frac{\kappa^2 T_Z^2}{(D^2 t^2 u^2)} \left[12m^{10}(n-2)tu + m^2 tu \{3(n-2)^2 t^4 \right. \\ &- 2[-68 + n(104 + (-31 + n)n)]t^3 u + 2[284 + n(-264 + (63 - 2n)n)]t^2 u^2 \\ &- 2[-68 + n(104 + (n - 31)n)]tu^3 + 3(n-2)^2 u^4 - 48m_z^6(n-2)(t+u) \\ &- 4m_z^4 [3(n-9)(n-2)t^2 + 2(124 + 3(n-21)n)tu + 3(n-9)(n-2)u^2] \\ &+ 4m_z^2(t+u)[3(n-5)(n-2)t^2 - 2(-90 + n(n+35))tu + 3(n-5)(n-2)u^2] \left. \right\} \\ &- 3m^8 \{12(n-2)tu(t+u) + m_z^2[(n-2)^2 t^2 + 2(16 + (n-14)n)tu \\ &+ (n-2)^2 u^2]\} - 3m^6 \{4m_z^4(18 + (n-13)n)tu - 2m_z^2(t+u)[(n-2)^2 t^2 \\ &+ 2(26 + n(2n-21))tu + (n-2)^2 u^2] - tu[(n-2)(10+n)t^2 \\ &+ 2(-32 + 3n(2+n))tu + (n-2)(10+n)u^2]\} \\ &+ 2t^2 u^2 \{32m_z^6(n-2) - 8m_z^4(-6 + n + n^2)(t+u) \\ &+ (40 + (n-17)n)(t+u)[(n-2)t^2 + 2(n-4)tu + (n-2)u^2] \end{aligned}$$

$$\begin{aligned}
& - m_z^2[(n-2)(48+(n-25)n)t^2 \\
& + 2(-156+n(118+(n-27)n))tu+(n-2)(48+(n-25)n)u^2]\} \\
& + m^4\{48m_z^6(n-2)tu+24m_z^4(18+(n-12)n)tu(t+u) \\
& - 6tu(t+u)[(n-2)nt^2+2(-12+n(3n-4))tu+(n-2)nu^2] \\
& - m_z^2[3(n-2)^2t^4+12(n-6)(3n-5)t^3u+2(604+n(25n-344))t^2u^2 \\
& + 12(n-6)(3n-5)tu^3+3(n-2)^2u^4]\}
\end{aligned} \tag{8}$$

where $D = (s - m_Z^2)$ and s, t, u are the usual Mandelstam invariants. The over all bar in LHS of eq. (8) represents that the matrix elements have been averaged over the spins and the colors of the initial state particles and summed over those of the final state ones.

2.2 Next-to-Leading Order Calculation

At the NLO in the perturbation theory, the cross sections receive $\mathcal{O}(\alpha_s)$ contributions from real emission as well as virtual diagrams. The integration over the phase space of the real emission diagrams will give rise to infra-red (IR) (soft and collinear) divergences in the limit where the additional parton at NLO is either soft and/or collinear to the initial state partons. On the other hand, the integration over the loop momenta in the virtual diagrams will also give rise to infrared divergences, in addition to the ultraviolet (UV) divergences. In our calculation, we regulate all these divergences using dimensional regularization with $n = 4 + \epsilon$ being the number of space time dimensions. Completely anti-commuting γ_5 prescription [22] is used to handle γ_5 in n dimensions. Here, it should be noted that as the gravitons couple to the energy momentum tensor of the SM fields, which is a conserved quantity, there won't be any UV divergences coming from the loop diagrams.

There are several methods available in the literature to compute NLO QCD corrections. Standard methods based on fully analytical computation deal with the phase space and loop integrals in n -dimensions and give a finite $\mathcal{O}(\alpha_s)$ contribution to the cross sections, after the real and the virtual contributions are added together and the initial state collinear singularities are absorbed into the bare parton distribution functions. However, these methods are not useful whenever the particles in the final state are subjected to either histogramming or experimental cuts or some isolation algorithms. In such cases, semi analytical methods like *phase space slicing method* or *dipole subtraction method* are extremely useful. In the present work, we have resorted to the former with two cut offs to compute the radiative corrections. In this method, the IR divergences appearing in the real diagrams can be handled in a convenient way by slicing the soft and collinear divergent regions from the full three body phase space. The advantage of this method is that the integration over the remaining phase space can be carried out in 4-dimensions, rather than in n -

dimensions, using standard Monte-Carlo techniques. In what follows, we give some of the details about the implementation of this phase space slicing method in our NLO computation.

2.2.1 Real Emission Processes

There are two types of subprocesses that contribute to the associated production of the vector gauge boson and the graviton at NLO in QCD. They proceed by $q\bar{q}$ and qg initial states. At parton level, the $2 \rightarrow 3$ quark anti-quark initiated subprocess is given by

$$q_a(p_1) + \bar{q}_b(p_2) \rightarrow V(p_3) + G(p_4) + g(p_5).$$

We find that 14 diagrams contribute to this subprocess and a few of them are depicted in Fig. 2. These diagrams are obtained by taking the t -channel $q\bar{q} \rightarrow Vg$ diagram at tree level and by attaching the graviton line to all the possible external as well as internal lines and to the vertices. The remaining diagrams are obtained by interchanging the vector boson and the graviton lines in Fig. 2. In general, diagrams

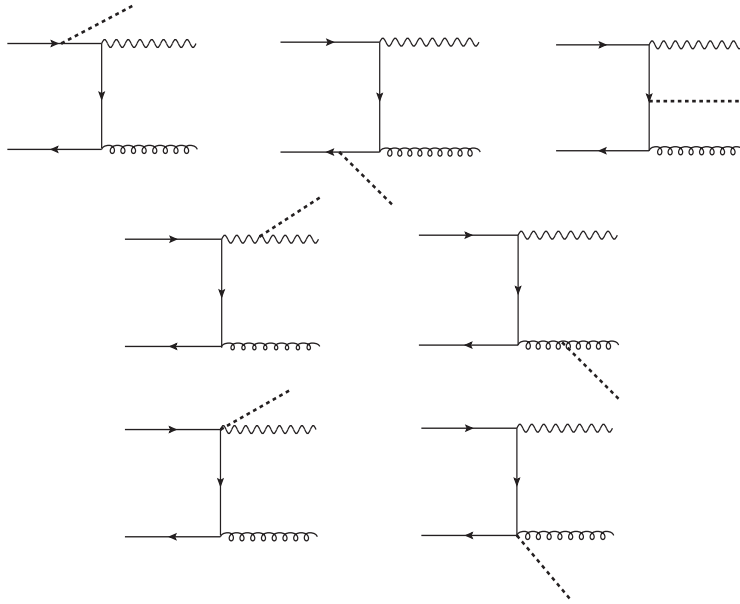


Figure 2: Real gluon emission diagrams

such as these involving gluons and massless quarks are prone to be singular in the soft and collinear regions of the 3-body phase space integration. In the phase space slicing method that we adopted here, these soft and collinear regions are separated from the full 3-body phase space using two small cut-off parameters, namely δ_s and δ_c , that define these singular regions. In the center of mass frame of the partons, the soft region is defined as: $0 \leq E_5 \leq \frac{1}{2}\delta_s\sqrt{s}$, where E_5 is the gluon energy and \sqrt{s} is the parton center of mass energy. Integration of the eikonal approximated $2 \rightarrow 3$

matrix elements over the soft region of the phase space gives the $\mathcal{O}(\alpha_s)$ 2-body contribution,

$$d\hat{\sigma}_S = a_s C_F F(\epsilon, \mu_R, s) \left(\frac{16}{\epsilon^2} + \frac{16}{\epsilon} \ln \delta_s + 8 \ln^2 \delta_s \right) d\hat{\sigma}_0 \quad (9)$$

where

$$F(\epsilon, \mu_R, s) = \left[\frac{\Gamma(1 + \frac{\epsilon}{2})}{\Gamma(1 + \epsilon)} \left(\frac{4\pi\mu_R^2}{s} \right)^{-\frac{\epsilon}{2}} \right], \quad C_F = \frac{N^2 - 1}{2N} \quad \text{and} \quad a_s = \frac{\alpha_s(\mu_R)}{4\pi}.$$

Here, $\alpha_s(\mu_R) = g_s^2(\mu_R)/4\pi$ with g_s being the running strong coupling constant, μ_R is the renormalization scale and N is the number of colors. The region complementary to that of the soft “ S ”, i.e. $E_5 > \frac{1}{2}\delta_s\sqrt{s}$, is defined as the hard region (H) of the phase space. Within this hard region “ H ”, the emitted gluon can be collinear to the incoming massless quark or anti-quark and hence can give rise to hard collinear divergences. By introducing another small cut-off parameter (δ_c), we separate these collinear divergences from the hard region. The hard collinear region (HC) can be defined as $:0 \leq -t_{ij} \leq \delta_c s$ ($i = 1, 2$ and $j = 5$), where $t_{ij} = (p_i - p_j)^2$. In the collinear limit, both the $2 \rightarrow 3$ matrix elements and the 3-body phase space get simplified to be expressed in terms of the born cross section as:

$$\begin{aligned} d\sigma_{HC}^{q\bar{q}} &= 4a_s d\hat{\sigma}_0 F(\epsilon, \mu_R, s) \left(\frac{1}{\epsilon} \right) \left\{ [P_{qq}(z, \epsilon) f_{q/P}(x_1/z) f_{\bar{q}/P}(x_2) + (q \leftrightarrow \bar{q})] \right. \\ &\quad \left. + (x_1 \leftrightarrow x_2) \right\} \frac{dz}{z} \left(\delta_c \frac{1-z}{z} \right)^{\frac{\epsilon}{2}} dx_1 dx_2 \end{aligned} \quad (10)$$

where $f_{a/P}(x)$ s’ are the bare parton distribution functions (PDF) and $P_{ab}(z, \epsilon)$ are the unregulated splitting functions in n -dimensions and are related to the usual Altarelli-Parisi splitting kernels as $P_{ab}(z, \epsilon) = P_{ab}(z) - \frac{\epsilon}{2} P'_{ab}(z)$ [23]. Here z denotes the fraction of the incoming parton b ’s momentum carried by the parton a . Note that for P_{qq} splitting in the hard region, since a fraction of the parton momentum i.e. δ_s is already carried away by the gluon, the effective limits of the integration for z will be $0 < z < 1 - \delta_s$.

Apart from the $q\bar{q}$ initiated subprocess at NLO, there will also be a $q(\bar{q})g$ initiated subprocess given by

$$q_a(p_1) + g(p_2) \rightarrow V(p_3) + G(p_4) + q_b(p_5).$$

Here the emitted parton, being a quark or an anti-quark instead of a gluon, won’t give rise to soft singularity. However, there will be hard collinear singularities whenever the emitted quark (anti-quark) becomes collinear to the incoming partons. These collinear singularities are separated using the cut-off δ_c in the same way as in

the case of $q\bar{q}$ initiated subprocess. The cross section in this collinear region turns out to be

$$d\sigma_{HC}^{qg,\bar{q}g} = 4a_s d\hat{\sigma}_0 F(\epsilon, \mu_R, s) \left(\frac{1}{\epsilon}\right) \left\{ [P_{\bar{q}g}(z, \epsilon) f_{q/P}(x_1) f_{g/P}(x_2/z) + (q \leftrightarrow \bar{q})] \right. \\ \left. + (x_1 \leftrightarrow x_2) \right\} \frac{dz}{z} \left(\delta_c \frac{1-z}{z}\right)^{\frac{\epsilon}{2}} dx_1 dx_2 \quad (11)$$

These initial state collinear divergences appearing in eqns. (10 & 11) as poles in ϵ are purely due to the massless nature of the partons involved in the scattering process. These divergences can be factored out from the parton level cross sections and be absorbed into the bare parton distribution functions at an arbitrary factorization scale μ_F , a process called mass factorization. In the \overline{MS} scheme, the scale dependent parton distribution functions, $f_{a/P}(x, \mu_F)$, can be expressed in terms of the bare parton distribution functions as given by

$$f_{a/P}(x, \mu_F) = f_{a/P}(x) + 2a_s \sum_b \left(\frac{1}{\epsilon}\right) F(\epsilon, \mu_R, \mu_F) \int_x^1 \frac{dz}{z} P_{ab}(z) f_{b/P}(x/z), \quad (12)$$

where $a, b = q(\bar{q}), g$. Substituting these parton densities in $d\hat{\sigma}_0$ produces collinear singular counter terms which when added with the hard collinear contributions results in the following $\mathcal{O}(a_s)$ contribution [10, 11]:

$$d\sigma_{coll} = 2a_s d\hat{\sigma}_0 F(\epsilon, \mu_R, s) \left\{ \left[f_{\bar{q}/p}(x_2, \mu_F) [\tilde{f}_{q/p}(x_1, \mu_F) + f_{q/p}(x_1, \mu_F)] \right. \right. \\ \left. \left. \left(-\frac{2}{\epsilon} + \ln \frac{s}{\mu_F^2} \right) A_{q \rightarrow q+g} \right] + (q \leftrightarrow \bar{q}) \right\} + (x_1 \leftrightarrow x_2) dx_1 dx_2 \quad (13)$$

where $A_{q \rightarrow q+g} = C_F (2 \ln \delta_s + \frac{3}{2})$. The tilde parton distribution functions are given by [14, 23]

$$\tilde{f}_{q/P}(x, \mu_F) = \sum_{b=q,g} \int_x^{1-\delta_s \delta_{qb}} \frac{dy}{y} f_{b/P}(x/y, \mu_F) \times \tilde{P}_{qb}(y) \quad (14)$$

$$\text{with } \tilde{P}_{ab}(y) = P_{ab}(y) \ln \left(\delta_c \frac{1-y}{y} \frac{s}{\mu_F^2} \right) - P'_{ab}(y). \quad (15)$$

Note that there is an additional factor of two, as the parton in the final state can be collinear to either of the incoming partons, which is implicit from $(q \leftrightarrow \bar{q})$ in eqn. (13). At this stage, one can observe that the divergent pieces that are proportional to $\ln \delta_s$ cancel among themselves. However, there are singularities still remaining that will get cancelled only with those coming from the loop integrals in the virtual diagrams. In what follows, we present the details of the virtual corrections to our process.

2.2.2 Virtual Corrections

The NLO cross sections also receive the contributions coming from the virtual corrections as well as the wave function renormalization to the $2 \rightarrow 2$ leading order processes. The corresponding Feynman diagrams are obtained by considering possible one loop virtual gluonic corrections to the tree level Feynman diagram for $q\bar{q} \rightarrow Z$ and then by attaching the graviton line to all possible internal as well as external lines and to vertices, as allowed by the Feynman rules. This way we find 27 diagrams, out of which 8 diagrams correspond to external leg corrections and can be omitted as they vanish in the massless quark limit. Out of the remaining 19 diagrams, 11 are shown in Fig. 3. The rest of the diagrams can easily be obtained by inverting the charge flow direction of the quark lines in the last eight diagrams shown in the Fig. (3). Interference of these one loop diagrams with the born diagrams gives

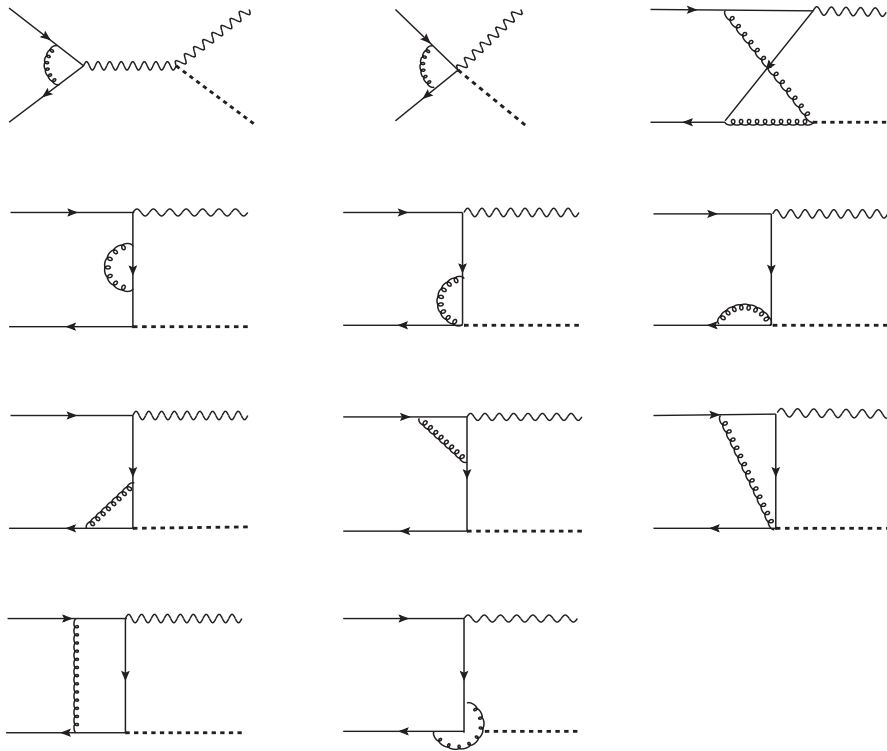


Figure 3: Virtual gluon emission diagrams

$\mathcal{O}(a_s)$ contributions. Due to tensorial interaction of gravitons with the SM fields the loop integrals involve higher powers of loop momenta in their numerators and hence the reduction of tensorial integrals to scalar ones becomes complicated. We have written a symbolic program using FORM [21] to perform this reduction in n dimensions. The resulting scalar integrals are then evaluated exactly (see [24]) and they are listed in the Appendix. Substituting these scalar integrals, we can express

the $\mathcal{O}(a_s)$ contribution resulting from the virtual processes as

$$\begin{aligned}
d\hat{\sigma}_V &= a_s d\hat{\sigma}_0 F(\epsilon, \mu_R, s) C_F \left(-\frac{16}{\epsilon^2} + \frac{12}{\epsilon} \right) \\
&+ C \left[V_1 \ln^2 \left(\frac{-t}{\mu^2} \right) + V_2 D_0^{fin}(p_1, k, q) + V_3 D_0^{fin}(p_2, k, q) \right. \\
&+ V_4 \ln^2 \left(\frac{-u}{\mu^2} \right) + V_5 \ln^2 \left(\frac{-m^2}{\mu^2} \right) + V_6 \ln^2 \left(\frac{-m_Z^2}{\mu^2} \right) + V_7 \ln^2 \left(\frac{s}{\mu^2} \right) \\
&+ V_8 \ln \left(\frac{-t}{\mu^2} \right) + V_9 \ln \left(\frac{-u}{\mu^2} \right) + V_{10} i C_0(k, q) + V_{11} + V_{12} + V_{13} \ln \left(\frac{m_Z}{\mu^2} \right) \\
&\left. + V_{14} \ln \left(\frac{m}{\mu^2} \right) + V_{15} \zeta_2 \right], \tag{16}
\end{aligned}$$

where $C = a_s \kappa^2 (C_v^2 + C_a^2) T_Z^2 C_F / (4N)$, C_0^{fin} and the D_0^{fin} s are the finite parts of the scalar integrals C_0 and D_0 respectively and are listed in the Appendix along with V_i s. It is clear from the above expression that the integration over the loop momenta in $4+\epsilon$ dimensions leads to soft and collinear singularities which appear as poles in ϵ . We found that the UV divergences that appear in the intermediate stages cancel among various diagrams thanks to the conservation of SM energy momentum tensor to this order in perturbation theory. Now, when we add $\mathcal{O}(\alpha_s)$ contributions coming from eq. (9), (13) and (16), we observe that the remaining soft and collinear singularities cancel among themselves as expected, leaving a finite expression for the 2-body contribution which can be computed using Monte-Carlo techniques. In other words, the 2-body contribution, given by

$$d\sigma^{2\text{-body}} = d\sigma_S + d\sigma_{coll} + d\sigma_V. \tag{17}$$

is found to be free of both UV and IR singularities and hence suitable for further numerical evaluation.

In addition to the above contribution, we also have the hard non-collinear region \overline{HC} of the phase space which do not suffer from any IR singularities by construction. The contributions from this region can be obtained by integrating the $2 \rightarrow 3$ matrix elements using standard Monte-Carlo integrations. Owing to the divergence free nature of the integration, the $2 \rightarrow 3$ matrix elements computed in 4-dimensions will suffice our purpose. These matrix elements are again computed using FORM. We have made several checks to ensure the correctness of our results, namely the gauge invariances in QCD, electroweak and gravity sectors. Since contributions from hard non-collinear regions involve three body phase space integrals of final state particles having different masses, care is needed to parameterize as well as to determine the limits of various integrations. We devote our next sub section to discuss this.

2.3 Three body contribution

In this section, we will present briefly how we have implemented various constraints imposed by the two cut off phase space slicing method and cuts on the phase space integrals for the $2 \rightarrow 3$ subprocesses. We are interested in the following cross section:

$$d\sigma^{3\text{-body}} = \int_{\overline{HC}, \text{cuts}} d\Gamma_3 |M_{q\bar{q}, qg}^{2\rightarrow 3}|^2. \quad (18)$$

where the three-body phase space measure is given by

$$d\Gamma_3 = \left(\prod_{i=1}^3 \frac{d^3 p_i}{(2\pi)^3 2E_i} \right) (2\pi)^4 \delta^{(4)}(p_1 + p_2 - p_3 - p_4 - p_5). \quad (19)$$

It is easy to parameterize all the momenta in the center of mass frame of initial state partons and then boost them to the lab frame or the center of mass frame of the hadrons. The 4-momenta of the massless partons in the initial state, moving along the z -axis, are given by

$$p_1 = \frac{\sqrt{s}}{2}(1, 0, 0, 1), \quad p_2 = \frac{\sqrt{s}}{2}(1, 0, 0, -1) \quad (20)$$

where \sqrt{s} is the parton center of mass energy. The corresponding 4-momenta of the massive particles in the final state are given by $p_i = (E_i, \vec{p}_i)$ with masses $m_i^2 = E_i^2 - |\vec{p}_i|^2$, for $i = 3, 4, 5$. For the three body case, it is easy to consider the momentum direction of one of the final state particles, say \vec{p}_5 , as the reference direction and then parameterize the other two momenta \vec{p}_3 and \vec{p}_4 with respect to this direction:

$$\vec{p}_5 = |\vec{p}_5| (\sin\theta, 0, \cos\theta) \quad (21)$$

where θ is the angle between \vec{p}_5 and the z -axis. The momentum of \vec{p}_3 can now be parameterized with respect to the direction of \vec{p}_5 and then followed by a rotation in the xz -plane by an angle of θ to get $\vec{p}_3 = (p_3^x, p_3^y, p_3^z)$ in the center of mass frame of the partons as given by

$$\begin{aligned} p_3^x &= |\vec{p}_3| (\cos\theta \cos\alpha \sin\beta + \sin\theta \cos\beta) \\ p_3^y &= |\vec{p}_3| \sin\alpha \sin\beta \\ p_3^z &= |\vec{p}_3| (\cos\theta \cos\beta - \sin\theta \cos\alpha \sin\beta) \end{aligned} \quad (22)$$

where α and β are the azimuthal and polar angles of \vec{p}_3 with respect to \vec{p}_5 . The 4-momentum of p_4 simply follows from the energy momentum conservation. The three body phase space in eqn.(19) can now be expressed in terms of the angular variables, using

$$\frac{d^3 p_i}{2E_i} = d^4 p_i \delta(p_i^2 - m_i^2) = \frac{|\vec{p}_i|}{2} dE_i d\Omega_i \quad (23)$$

to get

$$d\Gamma_3 = \frac{|\vec{p}_3||\vec{p}_5|}{4(2\pi)^5} dE_3 d\Omega_3 dE_5 d\Omega_5 \delta(p_4^2 - m_4^2), \quad (24)$$

where $d\Omega_3 = d\cos\beta d\alpha$ and $d\Omega_5 = d\cos\theta d\phi$. Further, the angle β can be eliminated using

$$2 |\vec{p}_3| |\vec{p}_5| \cos\beta = |\vec{p}_4|^2 - |\vec{p}_3|^2 - |\vec{p}_5|^2 \quad (25)$$

Finally, out of the nine integration variables of the three body phase space, in eqn.(19), we are left with four independent variables *viz.* E_3 , E_5 , θ and η , (due to 4-momentum conserving delta function and the rotational invariance of \vec{p}_5 , the reference momentum direction). The three body phase space can then be written in terms of these four independent variables as

$$d\Gamma_3 = \frac{1}{8(2\pi)^4} dE_3 dE_5 d\cos\theta d\eta \quad (26)$$

The limits of integration of E_3 and E_5 can be obtained from the constraint $|\cos\beta| \leq 1$, and are given by

$$E_5^{min} = m_5, \quad E_5^{max} = \frac{1}{2\sqrt{s}}[s + m_5^2 - (m_3 + m_4)^2] \quad (27)$$

and

$$E_3^{min,max} = \frac{1}{2\tau} \left[A(B + m_+ m_-) \pm \sqrt{(B - m_+^2)(B - m_-^2)} \right] \quad (28)$$

where

$$A = \sqrt{s} - E_5, \quad B = A^2 - |\vec{p}_5|^2 \quad \text{and} \quad m_{\pm} = m_3 \pm m_4 \quad (29)$$

Finally, all the parton momenta can be boosted back to the lab frame or the center of mass frame of the hadrons by a boost factor given, in the limit of the zero rest mass of the hadrons, by

$$\beta = \frac{P_{cm}}{E_{cm}} = \frac{(x_1 - x_2)}{(x_1 + x_2)} \quad (30)$$

where x_1 and x_2 are the fractions of the incoming hadron momenta carried by the partons in the center of mass frame of the hadrons.

We have implemented this phase space parameterization in our numerical code written in Fortran 77. We set $p_i = k_i$ ($i = 3, 4, 5$) and $m_3 = m_V, m_4 = m$ in our code. Here m_V is mass of the gauge boson and m is mass of the graviton. The phase space integrations as well as various convolutions in the two and three body contributions are done using VEGAS multi dimensional integration package. In what follows, we present the impact of our NLO corrections on various observables.

3 Numerical Results

3.1 Neutral gauge bosons

In this section, we present various kinematic distributions for the associate production of the graviton and the vector gauge boson to NLO in QCD at the LHC. The results are presented for proton-proton collision energy of $\sqrt{S} = 14$ TeV. As discussed before, the inclusive cross section for the graviton production involves the summation of all possible graviton modes. This summation in the continuum limit leads to an integral over the graviton mass. The limits of this integral are set by the kinematics from 0 to $\sqrt{s} - m_V$, where \sqrt{s} is the parton center of mass energy and $m_V = m_Z, m_W$. The masses of the gauge bosons and the weak mixing angle are given by [25]

$$m_Z = 91.1876 \text{ GeV}, \quad m_W = 80.398 \text{ GeV}, \quad \sin^2\theta_w = 0.2312 \quad (31)$$

The fine structure constant is taken to be $\alpha = 1/128$. Throughout our study, we have used CTEQ6L1 and CTEQ6.6M parton density sets [26] for LO and NLO cross sections respectively. The strong coupling constant is calculated at two loop order in the \overline{MS} scheme with $\alpha_s(m_Z) = 0.118$ ($\Lambda_{\text{QCD}} = 0.226$ GeV). We have also set the number of light flavors $n_f = 5$. The following cuts are used for our numerical study,

$$p_T^{Z,W} > p_T^{\text{min}}, \quad p_T^{\text{miss}} > p_T^{\text{min}}, \quad |y^{Z,W}| \leq 2.5. \quad (32)$$

For the 2-body process, the missing transverse momentum is same as that of the gauge boson. On the other hand, for the 3-body process, it need not be so due to the presence of an observable jet in the final state and hence it amounts purely to the graviton transverse momentum. The observable jet is defined as the one that satisfies the following conditions:

$$p_T^{\text{jet}} > 20\text{GeV} \quad \text{and} \quad |\eta^{\text{jet}}| \leq 2.5 \quad (33)$$

Whenever the jet does not satisfy the above conditions, the missing transverse momentum is approximated to be that of the gauge boson.

The LED model is an effective field theory valid below the UV cut-off scale M_s , which is expected to be of the order of a few TeV. At the LHC energies ($\sqrt{S} = 14$ TeV), it is very well possible that the partonic center of mass energies can exceed this scale M_s and lead to the signals that do not correspond to the compactified extra dimensions of the LED model. This necessitates the need to quantify the UV sensitivity of the theory and this issue was already addressed in [3], according to which the cross sections can be computed in two different ways, one with *truncation* where the cross sections are set to zero whenever the hard scale Q involved in the problem exceeds M_s , and the other with *un-truncation* where there is no such constraint imposed on the cross sections. As pointed out in [3], if these two results converge then the predictions are valid and the model is viable, otherwise the un-truncated cross sections can dominate the truncated ones, implying the calculations

are not under control. In our calculation, we choose the hard scale to be the invariant mass of the gauge boson and the graviton, $Q = M_{ZG}$, which at LO is the same as the center of mass energy of the partons \sqrt{s} . We will consider both truncated as well as un-truncated cases, however, most of our distributions are obtained with our default choice of truncation scheme.

Before proceeding to the kinematic distributions, we will do some consistency checks on the calculation. First, we check for the stability of the cross sections against the variation of the slicing parameters, δ_s, δ_c . The sum of the 2-body and the 3-body contributions given in eqns. (17) and (18) is expected to be independent of the choice of these slicing parameters that are introduced in the intermediate stages of the calculation. In fig.(4), we show the dependency of the transverse momentum distribution p_T^Z on the slicing parameter δ_s keeping the ratio of δ_s to δ_c , fixed at a value of 100. This distribution is obtained using the hard truncation scheme for a particular choice of the model parameters $M_s = 3$ TeV and $\delta = 4$. It can be seen from the fig.(4) that both the 2-body and the 3-body contributions vary with δ_s but their sum is fairly stable against the variation of δ_s over a wide range. This ensures the proper implementation of the slicing method in our NLO computation.

Another useful check on the computation is to reproduce the cross sections for the associated production of the photon and the graviton at the LHC [14]. In order to do this, we recalculated both real emission as well as virtual contributions for this process and the corresponding soft and collinear pieces. We found that the following replacements

1. $\frac{(C_V^2 + C_A^2)}{4} \rightarrow Q_f^2$
2. $m_z \rightarrow 0$
3. $T_z \rightarrow e$

in the two body and three body real emission matrix elements of the Z/W^\pm boson with Graviton production processes correctly reproduce the corresponding matrix elements for photon with Graviton production processes. Here, Q_f is the charge of the fermion and e is the electromagnetic coupling. Using our symbolic program, the analytical expression for virtual contributions for this process agrees with one given in the appendix of [14]. In addition, using these recalculated quantities, we reproduced all the numerical results in [14] after taking their choice of parameters, cuts etc. It is important to note that the NLO cross sections, or the K-factors, are subject to the choice of the event selection or more precisely the cuts on the particles in the final state. In our calculation, however, the gauge bosons being massive, we present our results according to the cuts given in eqns. (32 & 33).

In fig.(5), the total cross section for the associated production of Z -boson and the graviton is shown as a function of P_T^{min} , to NLO in QCD at the LHC. The cross sections are given for both the truncated as well as the un-truncated cases and with

the choice of model parameters $M_s = 3$ TeV and $d = 2$. A similar plot is shown for $d = 4$ in fig.(6). The K-factors are found to have a mild dependency on P_T^{min} , varying from 1.6 to 1.4. In fig.(7), we have shown the variation of the truncated as well as un-truncated total cross sections with respect to the scale M_s , for the case $d = 2$. The difference between the truncated and the un-truncated cross sections is mainly due to the contributions coming from the region $Q > M_s$. However, with increasing M_s the parton fluxes corresponding to Q in this region rapidly fall down and hence the difference between the two cross sections decreases with increase in M_s . Such a behavior is evident from the figures. (7) and (8), for $d = 2$ and $d = 4$ respectively. The corresponding K-factors are also shown in fig. (9). In the rest of our calculation we choose $P_T^{min} = 400$ GeV and $M_s = 3$ TeV.

Next, we present LO and NLO transverse momentum distributions of the Z -boson (P_T^Z) in fig.(10) for $d = 2, 4, 6$ and the corresponding missing transverse momentum distributions (P_T^{miss}) in the left panel of fig.(11) for $d = 2, 4$. The QCD corrections enhance both P_T^Z and P_T^{miss} distributions. Note that the shape of the P_T^Z distribution remains unaffected while this is not the case for P_T^{miss} distribution. Such a pattern can be understood from the definition of P_T^{miss} mentioned before.

Next, we present the rapidity distributions of Z bosons. The rapidity of massive gauge bosons is defined by

$$Y = \frac{1}{2} \log \left(\frac{E + p_z}{E - p_z} \right), \quad (34)$$

where E and p_z are the energy and the longitudinal momentum components of the gauge boson in the lab frame. In the right panel of fig.(11), we have plotted the rapidity distribution of the Z -boson both at LO and at NLO for two different choices of the factorization scale: $\mu_F = P_T^Z/2$ and $2P_T^Z$. This distribution is obtained by integrating over the transverse momentum of the Z -boson from 700 GeV to 750 GeV, for $d = 4$. Note that the NLO corrections increase the cross section. As expected, the inclusion of order a_s corrections reduces the dependence on the arbitrary factorization scale μ_F . The percentage of uncertainty in the cross sections at the central rapidity region $Y = 0$, due the variation of the scale from $\mu_F = P_T^Z/2$ to $\mu_F = 2P_T^Z$, is 18.9 at LO and it gets reduced to 8.6 at NLO.

3.2 Charged gauge bosons

In this section we discuss the impact of NLO QCD corrections on the associated production of charged gauge bosons (W^\pm) and the graviton at the LHC. The matrix elements for the W^\pm case are identical to those for the Z -boson case but for the masses of the gauge bosons and their couplings to the quarks as seen in eqn. (6). Further, in the case of charged gauge bosons, the parton fluxes will also be different from those of the neutral gauge boson. The parton fluxes for the quark anti-quark annihilation process in the case of Z -boson are of the form $q\bar{q}$ ($q = u, d, s, c, b$), while they are of the form $u\bar{d}$ ($d\bar{u}$) for W^+ (W^-). For W boson production cross sections,

we will consider the mixing of quarks among different quark generations, as allowed by the CKM-matrix elements V_{ij} , with $(i = u, c, t)$ and $(j = d, s, b)$. In view of this, in the above parton fluxes, u and d correspond to any up -type and $down$ -type quarks respectively. The CKM matrix elements are given by [25]

$$\begin{aligned} |V_{ud}| = 0.97425 \quad |V_{us}| = 0.2252 \quad |V_{ub}| = 3.89 \times 10^{-3} \\ |V_{cd}| = 0.230 \quad |V_{cs}| = 1.023 \quad |V_{cb}| = 40.6 \times 10^{-3} \end{aligned} \quad (35)$$

Since all our calculations are done in the massless limit of the partons, we have not included the top quark contribution in our calculation and set all V_{tj} 's to zero.

Similar to the case of Z boson, we will present the total cross sections as well as the differential distributions for the associated production of W^\pm boson and a graviton. In fig.(12) and fig.(20), we have shown the stability of the transverse momentum distributions of W^- and W^+ respectively, with the slicing parameter δ_s . These distributions are obtained for the choice of $P_T^W = 500$ GeV, keeping the ratio δ_s/δ_c fixed at 100. It can be seen from the figures that the sum of the 2-body and 3-body contributions is fairly stable against the variation of the slicing parameters. This ensures the proper implementation of the slicing method in our numerical code, taking into account the appropriate parton fluxes for W^\pm . Next, we present the total cross sections as a function of P_T^{min} as well as M_s . In fig.(13) and fig.(14), we show truncated as well as untruncated total cross sections for W^- case, as a function of P_T^{min} , for $d = 2$ and $d = 4$ respectively. It can be seen from these figures that the QCD corrections have enhanced the leading order cross sections considerably, but there is no significant change in the shape of the cross sections. Similar plots are shown for W^+ in fig.(21) and fig.(22).

In fig.(15) and fig.(16), we show the total cross sections for W^- as a function of M_s for $d = 2$ and $d = 4$, respectively. A set of similar plots for W^+ are shown in fig.(23) and fig.(24). Note that, in each of the above, the cross sections for W^+ are somewhat higher than the corresponding ones for W^- . This difference in the total cross sections can be understood from the respective parton fluxes for W^- and W^+ at the LHC. The corresponding K-factors are shown in fig.(17) for W^- and in fig.(25) for W^+ . For the choice of the parameters we have considered, the K-factors are found to vary from 1.7 to 1.4 in the case of W^- while they range from 1.65 to 1.05 for W^+ . Note that the K-factors for W^- case are comparable but a little higher than those for W^+ , which again can be accounted for the differences in the parton fluxes. The fact that the valence quark contributions are negligible and the parton fluxes at LO for W^+ are higher compared to those for W^- explains the behavior the above factors.

Further, in figs.(18) and (26), we present the transverse momentum distribution of W^- and W^+ respectively as a function of the number of extra dimensions d and for $M_s = 3$ TeV. Similarly, we show the missing transverse momentum distribution the graviton when produced in association with W^- in the left panel of fig.(19). In the right panel, we present the scale uncertainties in the rapidity distribution of W^-

by varying the factorization scale from $\mu_F = P_T^{W^-}/2$ to $\mu_F = 2P_T^{W^-}$. This rapidity distribution is obtained by integrating over the transverse momentum $P_T^{W^-}$ from 700 GeV to 750 GeV. Similar plots are shown for W^+ in fig.(27). Note that the uncertainty resulting from the factorization scale μ_F get reduced as we include order a_s corrections. The percentage of uncertainty at the central rapidity $Y^{W^\pm} = 0$ is decreased from 19.1 to 9.3 in the case of W^- , whereas it gets reduced from 18.8 to 8.3 in the case of W^+ .

4 Conclusions

In this paper, we have systematically computed the full NLO QCD corrections to the associated production of the vector gauge boson and the graviton in theories with large extra dimensions at the LHC. This process plays an important role in probing the extra dimensions at the collider experiments, thanks to the large parton fluxes available at the LHC. We have used a semi-analytical two cut-off phase space slicing method to compute these corrections. We have quantified the ultraviolet sensitivity of the theoretical predictions by studying the cross sections in the truncated as well as the untruncated cases. In both the cases, the radiative corrections are found to have enhanced the cross sections significantly but do not appreciably change their shapes. The K-factors for the neutral gauge boson are found to vary from 1.6 to 1.2 depending on the number of extra dimensions d , while they vary from 1.8 to 1.3 for the case of charged gauge bosons. Although, the choice of the model parameters has the potential to change the cross sections calculated in truncated or untruncated cases significantly, we notice that the K-factors remain almost the same in these two cases. In addition to the total cross sections, we have also studied the differential distributions of the vector gauge bosons and found that the radiative corrections are significant and they do not affect their shapes except for the missing transverse momentum distribution. At the hadron colliders, the leading order predictions often suffer from large uncertainties resulting from the choice of factorization scale. Reducing these uncertainties is one of the main motivations for doing NLO computation. We have shown that this is indeed the case for the rapidity distributions of the gauge bosons by varying the factorization scale from $\mu_F = P_T/2$ to $\mu_F = 2P_T$, leading to reduction in the percentage of scale uncertainty to 9% from 19%. Hence, the results presented in this paper are more suitable for studies on associated production of vector boson and graviton in the context of extra dimension searches at the hadron colliders.

Acknowledgments

The work of V.R. and M.C.K. has been partially supported by funds made available to the Regional Centre for Accelerator based Particle Physics (RECAPP) by the Department of Atomic Energy, Govt. of India. We would like to thank the cluster

computing facility at Harish-Chandra Research Institute where part of computational work for this study was carried out. S.S. would like to thank UGC, New Delhi for financial support. S.S. would also like to thank RECAPP center for his visit, where part of the work was done.

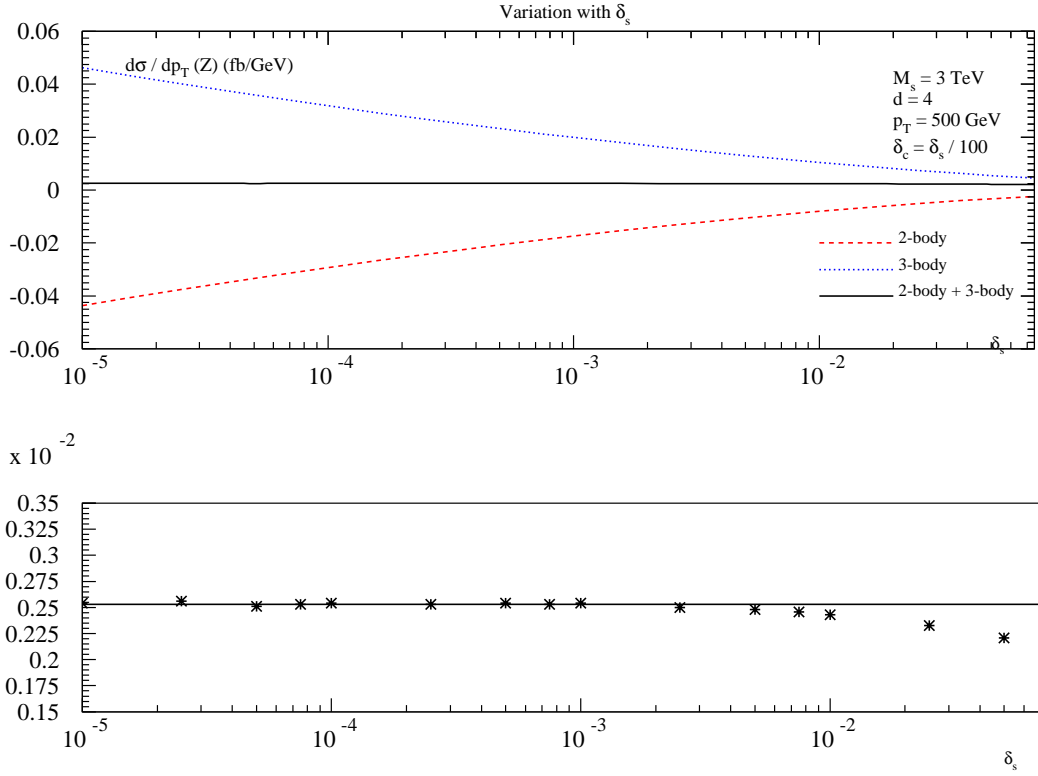


Figure 4: Variation of the transverse momentum distribution of Z boson with δ_s , keeping the ratio $\delta_s/\delta_c = 100$ fixed, for $M_s = 3$ TeV and $d = 4$.

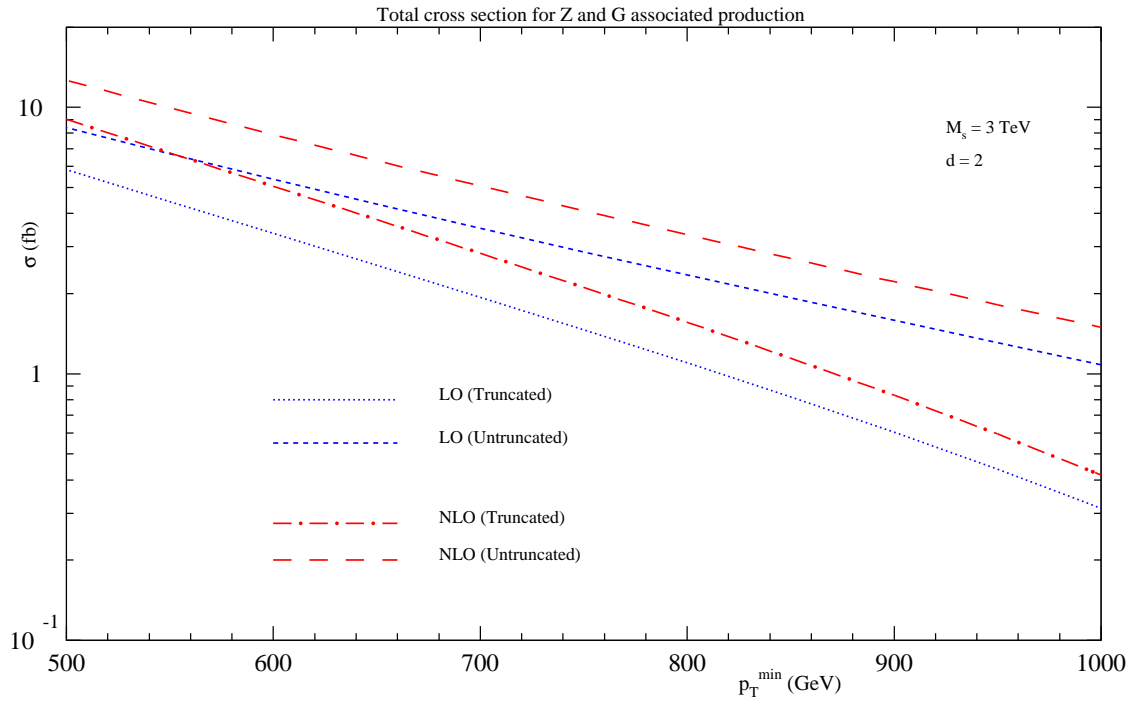


Figure 5: Total cross section for the associated production of Z and G as a function of P_T^{\min} at the LHC, for $M_s = 3 \text{ TeV}$ and $d = 2$.

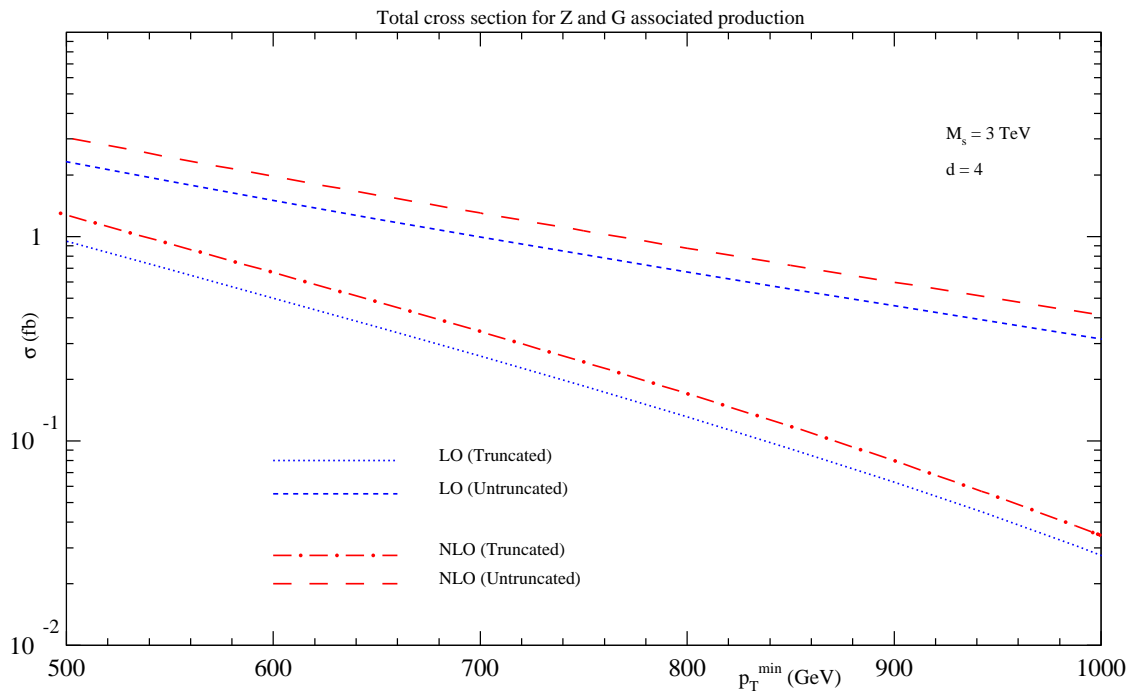


Figure 6: Total cross section for the associated production of Z and G as a function of P_T^{\min} at the LHC, for $M_s = 3 \text{ TeV}$ and $d = 4$.

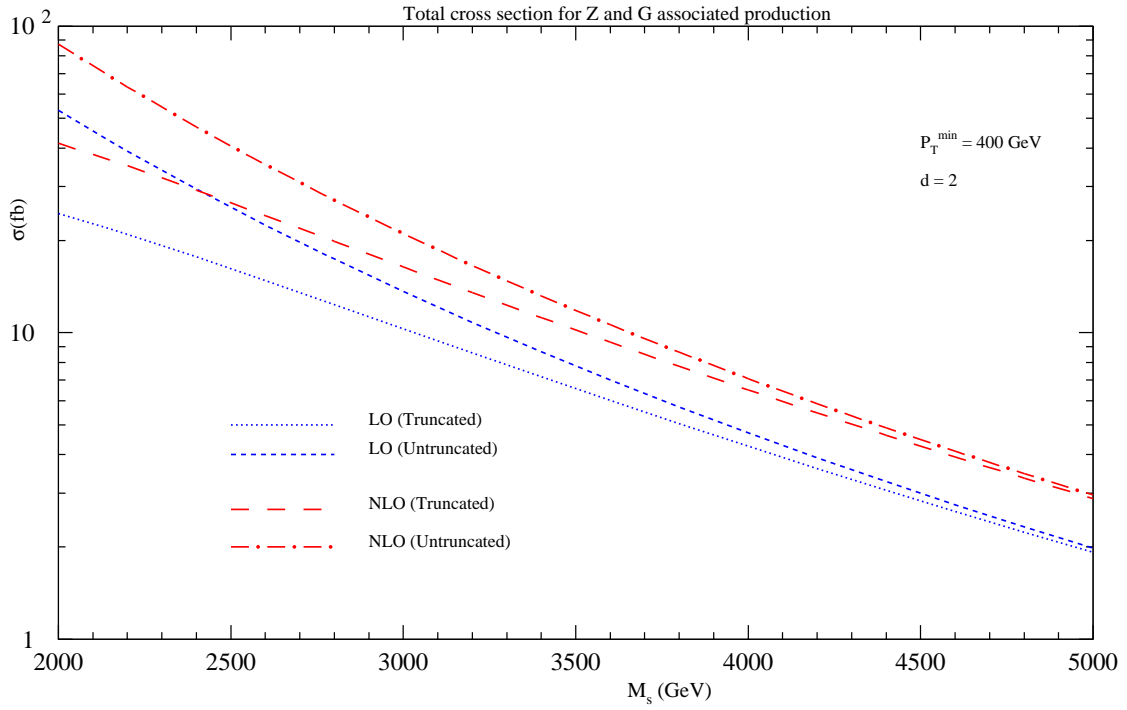


Figure 7: Total cross section for the associated production of Z -boson and the graviton at the LHC, shown as a function of M_s for $d = 2$.

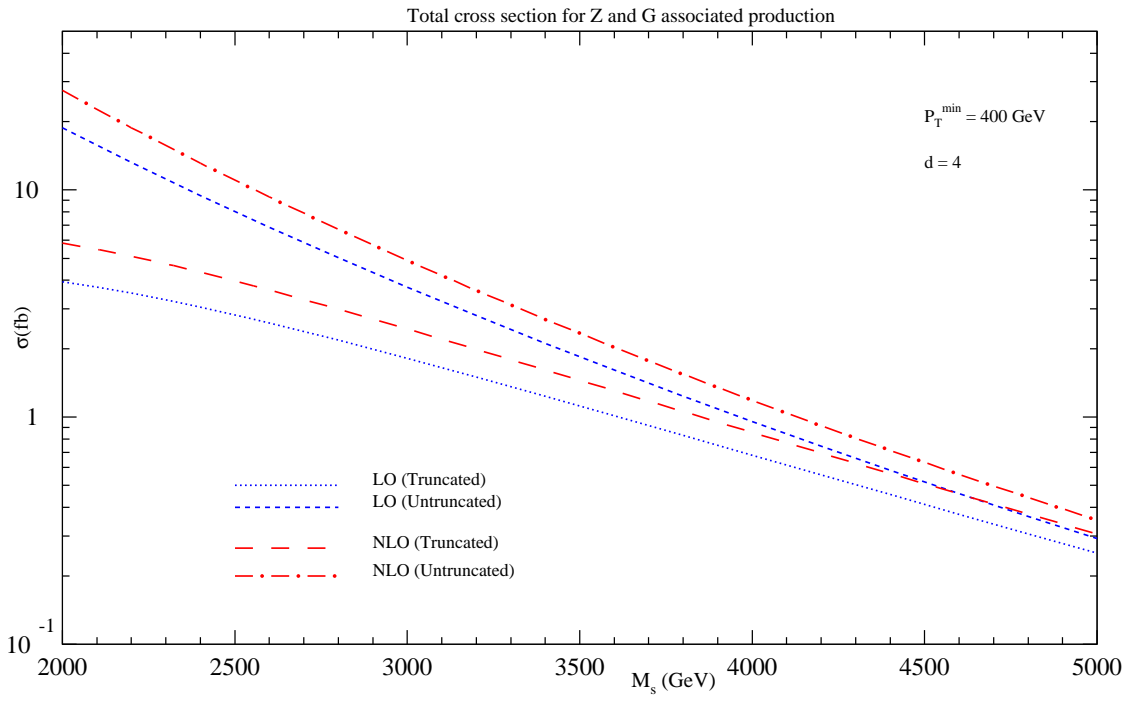


Figure 8: Total cross section for the associated production of Z -boson and the graviton at the LHC, shown as a function of M_s for $d = 4$.

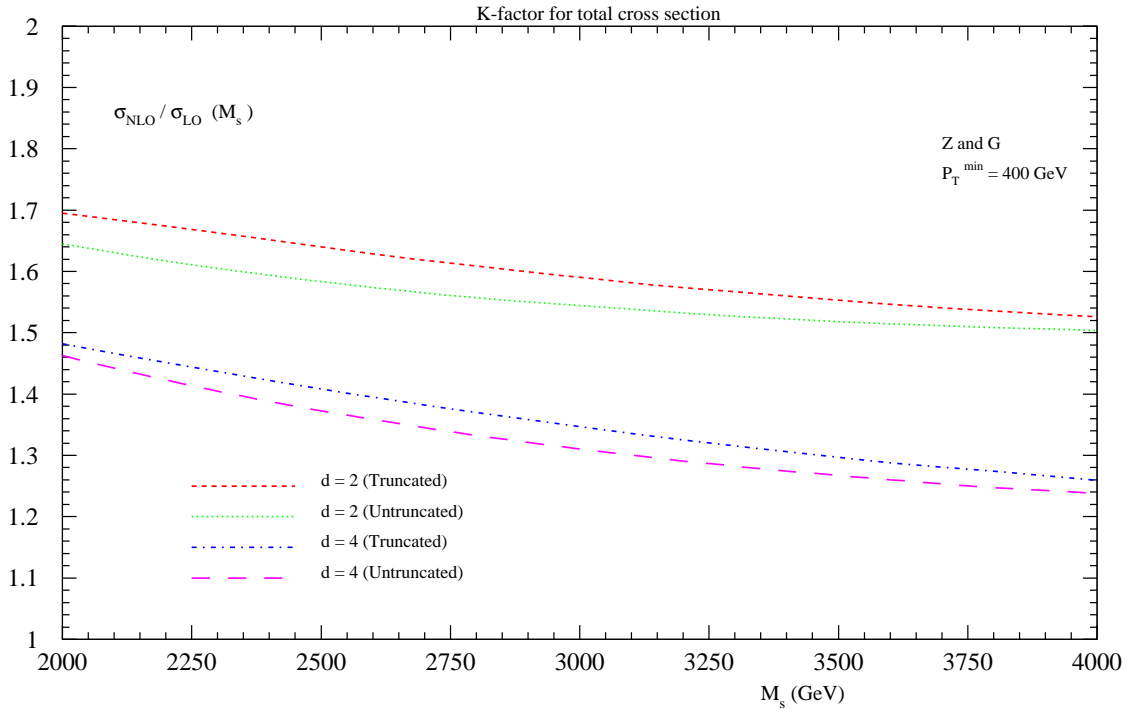
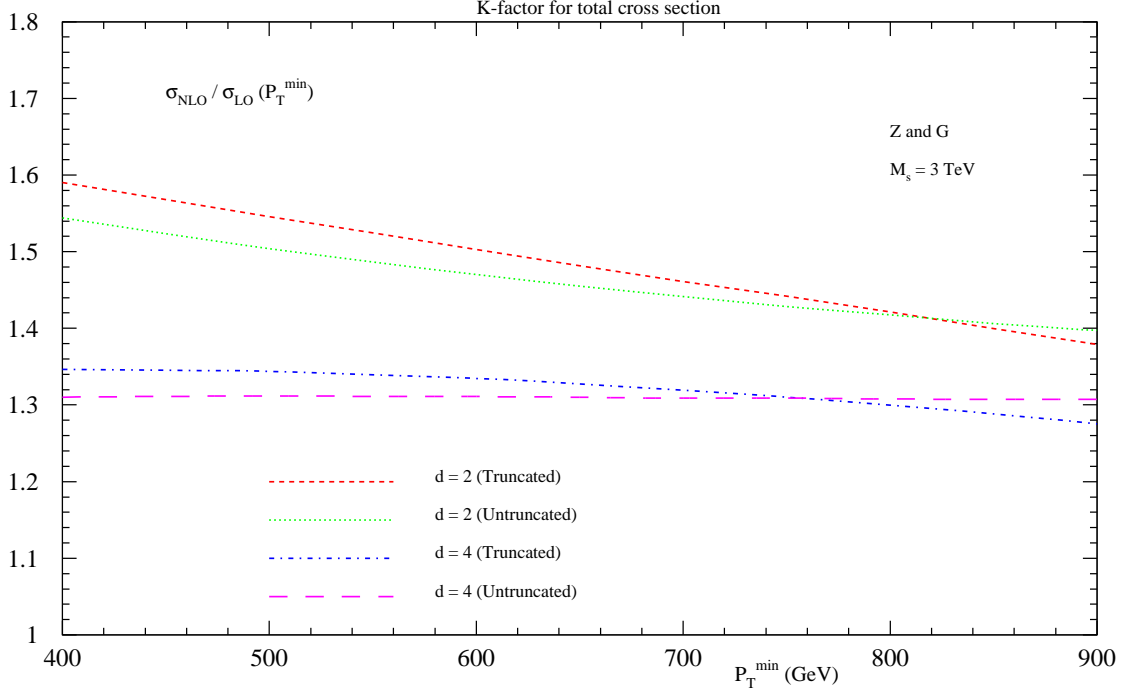


Figure 9: K-factors of the total cross section for the associated production of the Z -boson and the graviton at the LHC, given as a function of P_T^{min} (top) and the scale M_s (bottom).

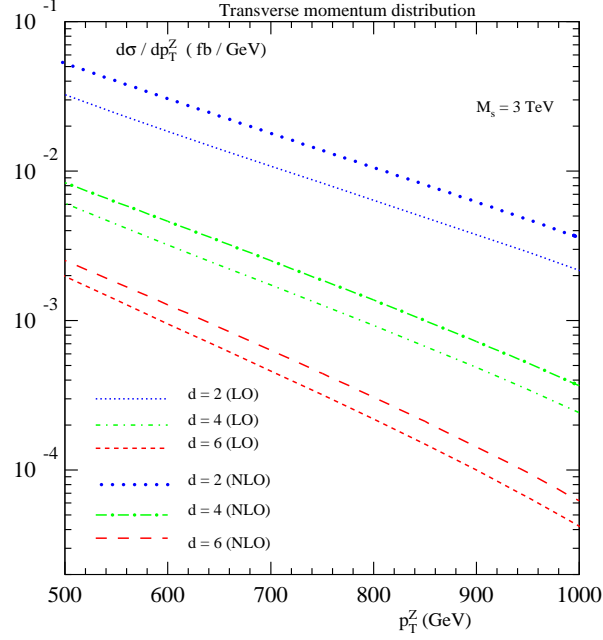


Figure 10: Transverse momentum distribution of the Z -boson for $M_s = 3$ TeV is shown for different values of the number of extra dimensions d .

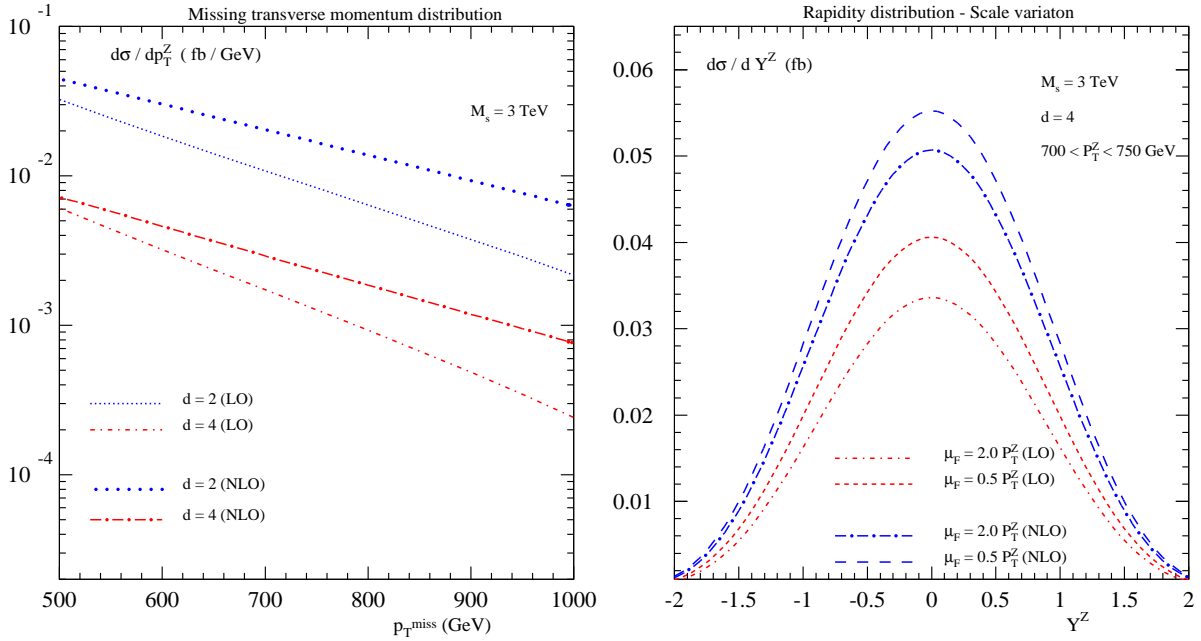


Figure 11: Missing transverse momentum distribution of the graviton produced in association with Z -boson at the LHC, for $M_s = 3$ TeV (left). The scale uncertainties in the rapidity distribution of Z -boson for $M_s = 3$ TeV and $d = 4$ (right).

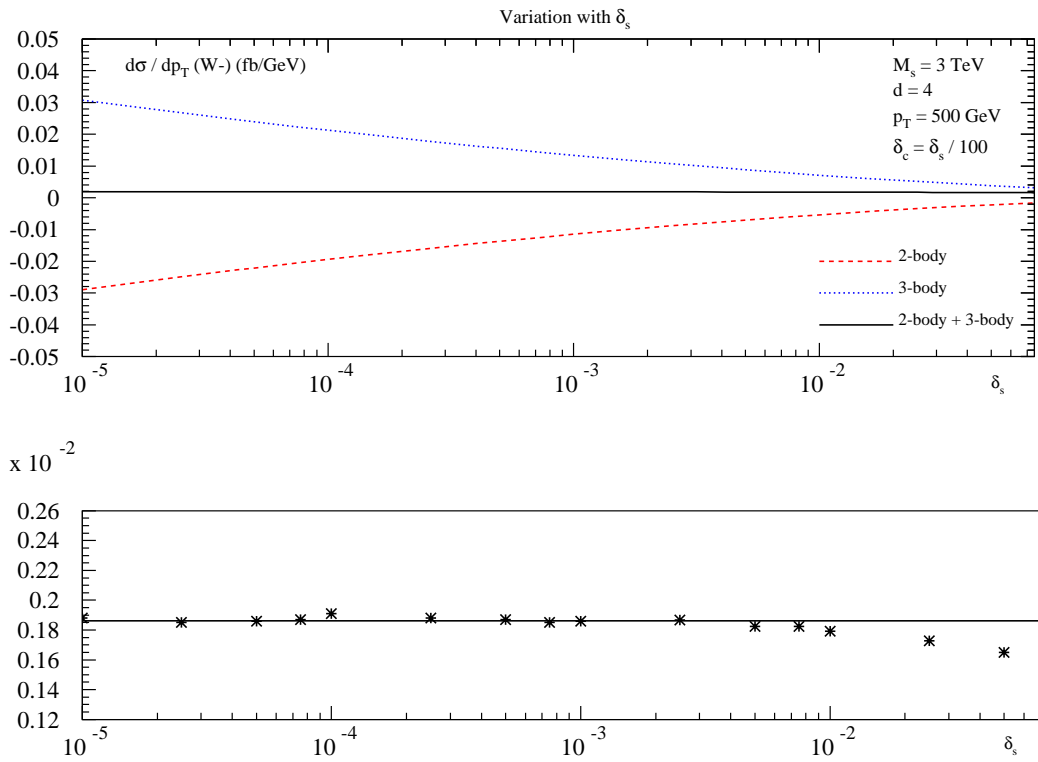


Figure 12: Variation of the transverse momentum distribution of W^- boson with δ_s , keeping the ratio $\delta_s/\delta_c = 100$ fixed, for $M_s = 3$ TeV and $d = 4$.

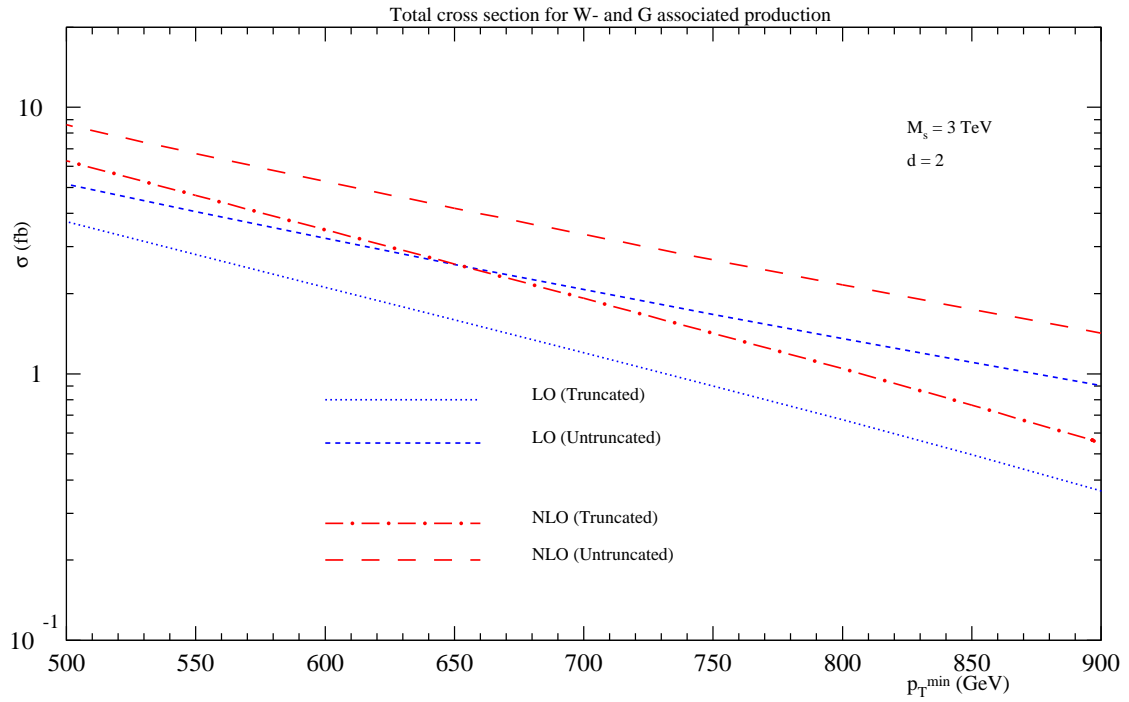


Figure 13: Total cross section for the associated production of W^- boson and the graviton at the LHC, as a function of P_T^{min} for $M_s = 3 \text{ TeV}$ and $d = 2$.

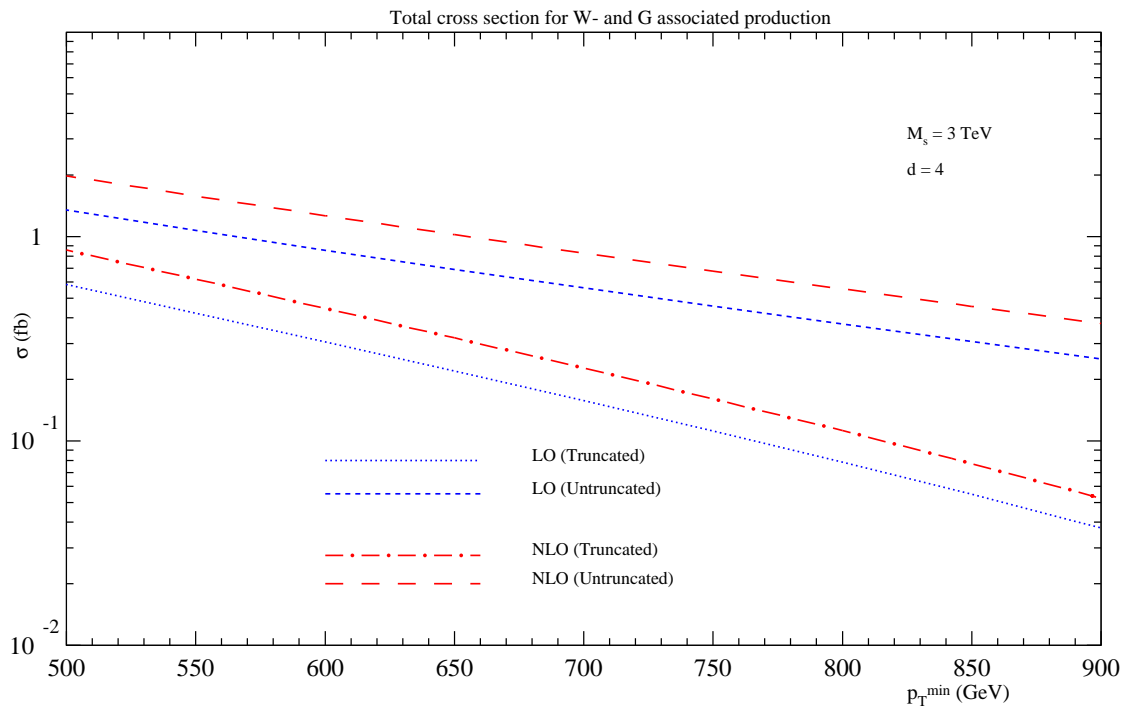


Figure 14: Total cross section for the associated production of W^- boson and the graviton at the LHC, shown as a function of P_T^{\min} for $M_s = 3 \text{ TeV}$ and $d = 4$.

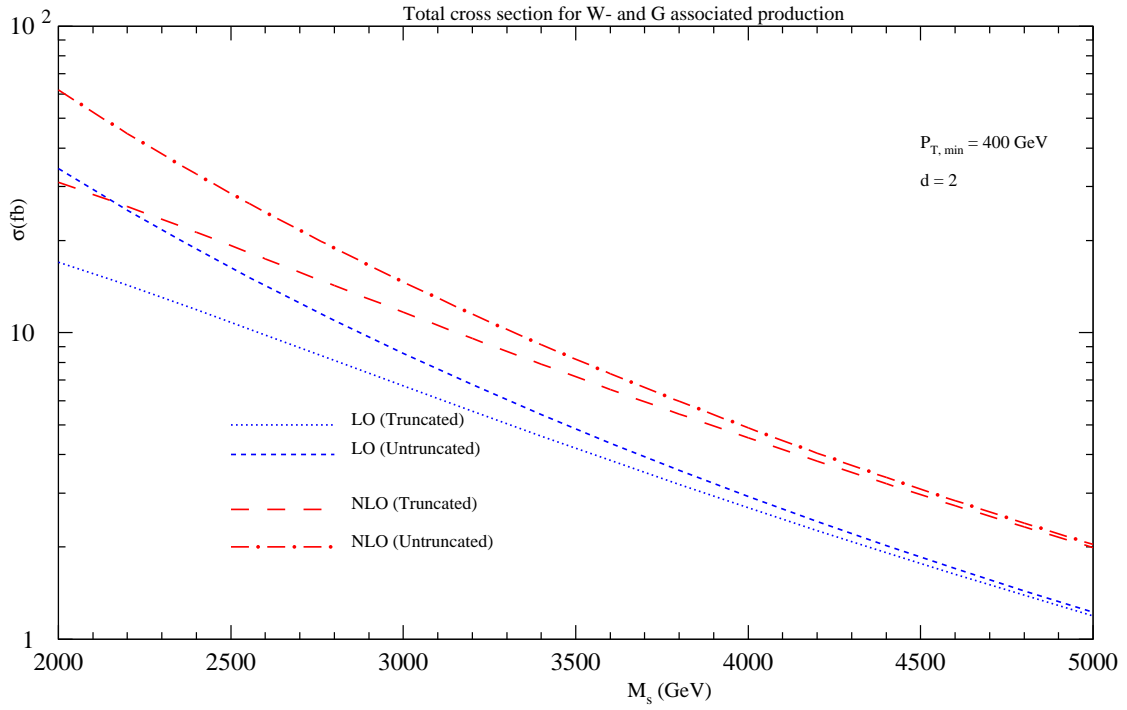


Figure 15: Total cross section for the associated production of W^- boson and the graviton at the LHC, given as a function of M_s for $d = 2$.

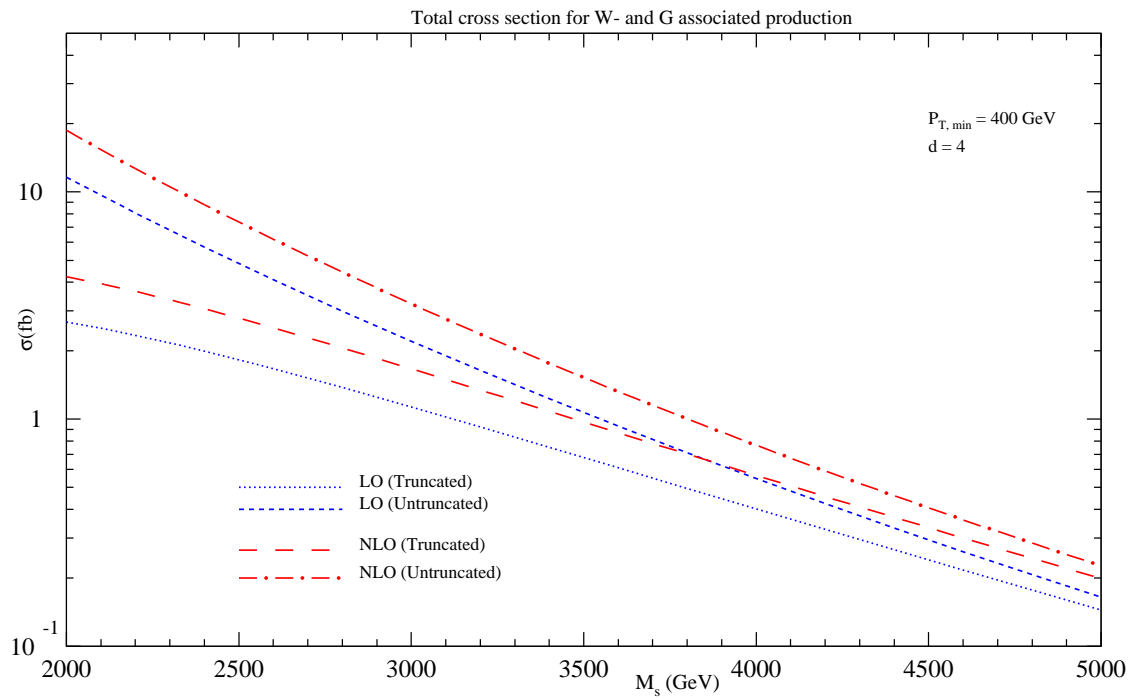


Figure 16: Total cross section for the associated production of W^- boson and the graviton at the LHC, shown as a function of M_s for $d = 4$.

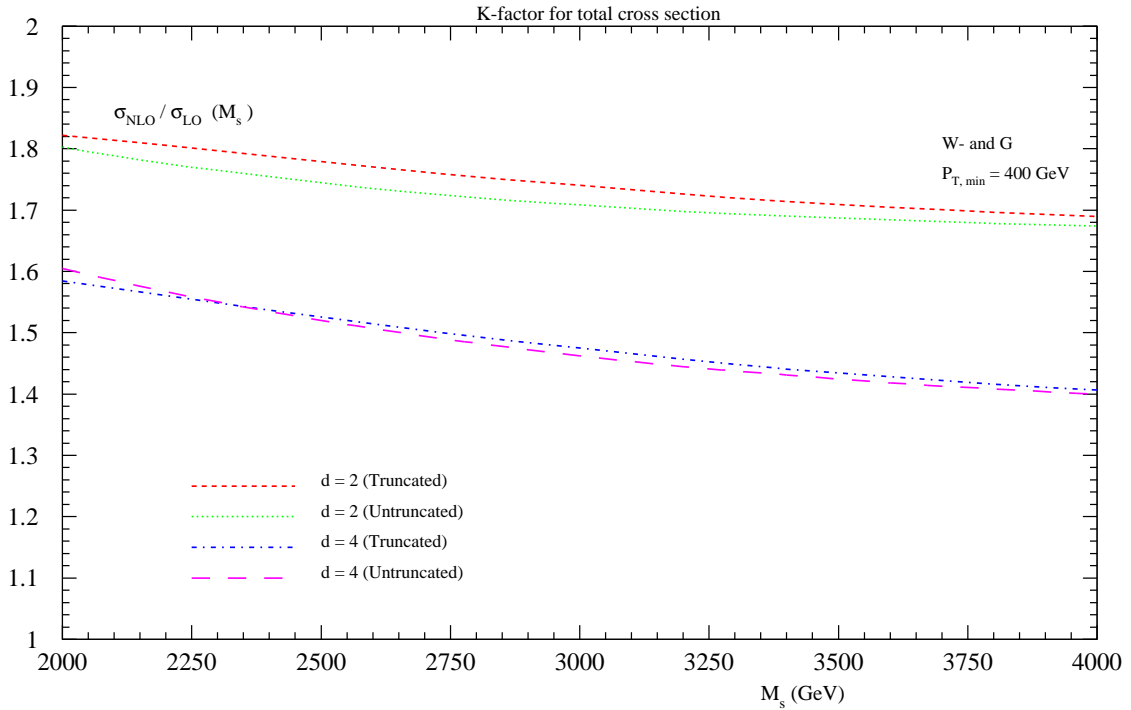
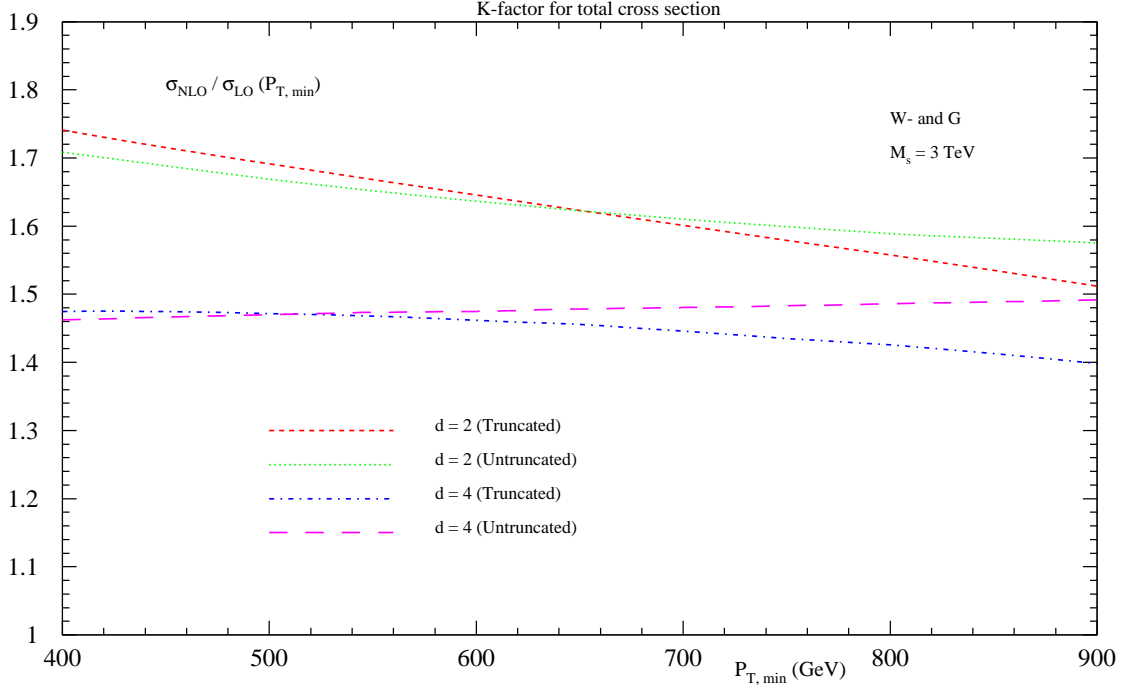


Figure 17: K-factors of the total cross section for the associated production of W^- boson and the graviton at the LHC, given as a function of P_T^{min} (top) and the scale M_s (bottom).

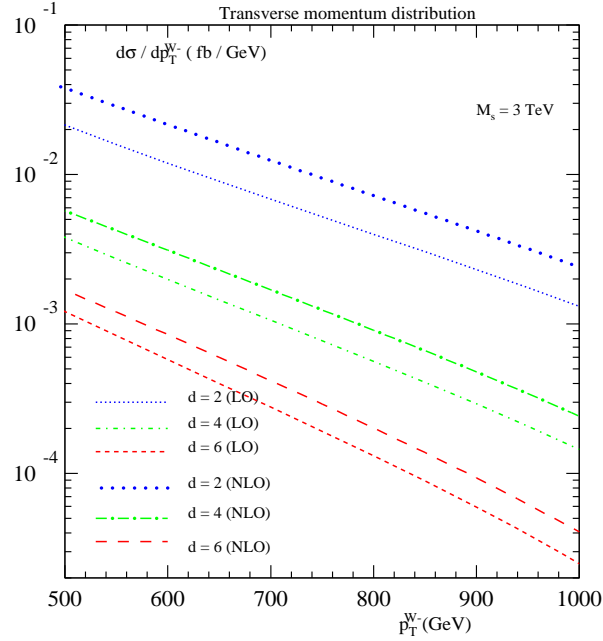


Figure 18: Transverse momentum distribution of the W^- -boson for $M_s = 3$ TeV is shown for different values of the number of extra dimensions d .

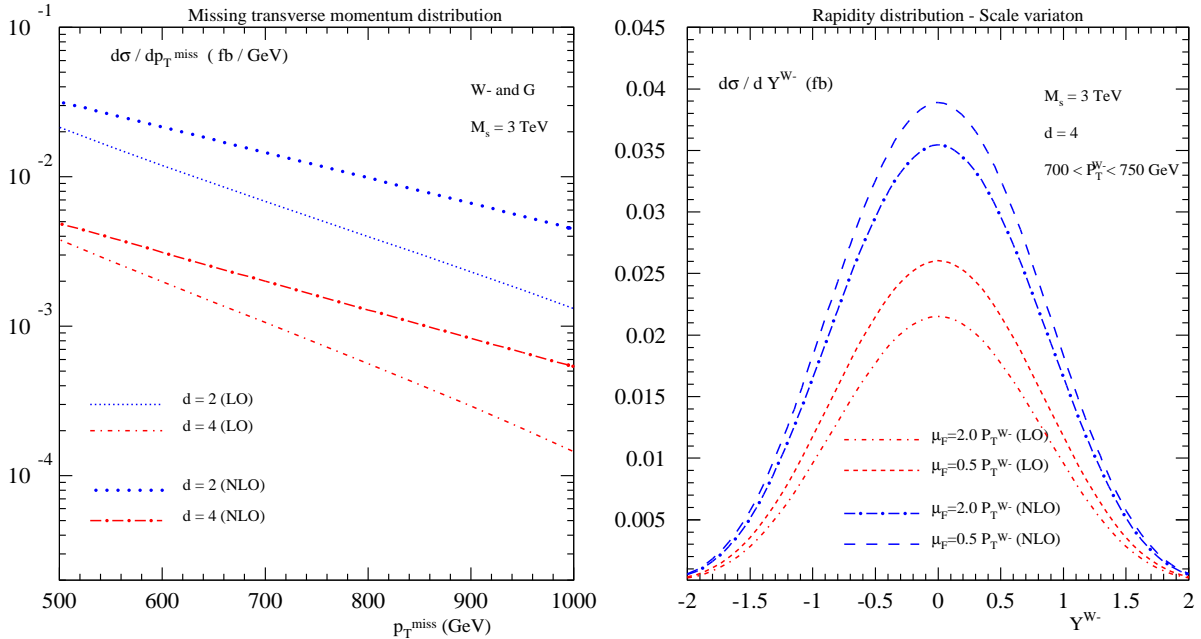


Figure 19: Missing transverse momentum distribution of the graviton produced in association with W^- -boson at the LHC, for $M_s = 3$ TeV (left). The scale uncertainties in the rapidity distribution of W^- boson for $M_s = 3$ TeV and $d = 4$ (right).

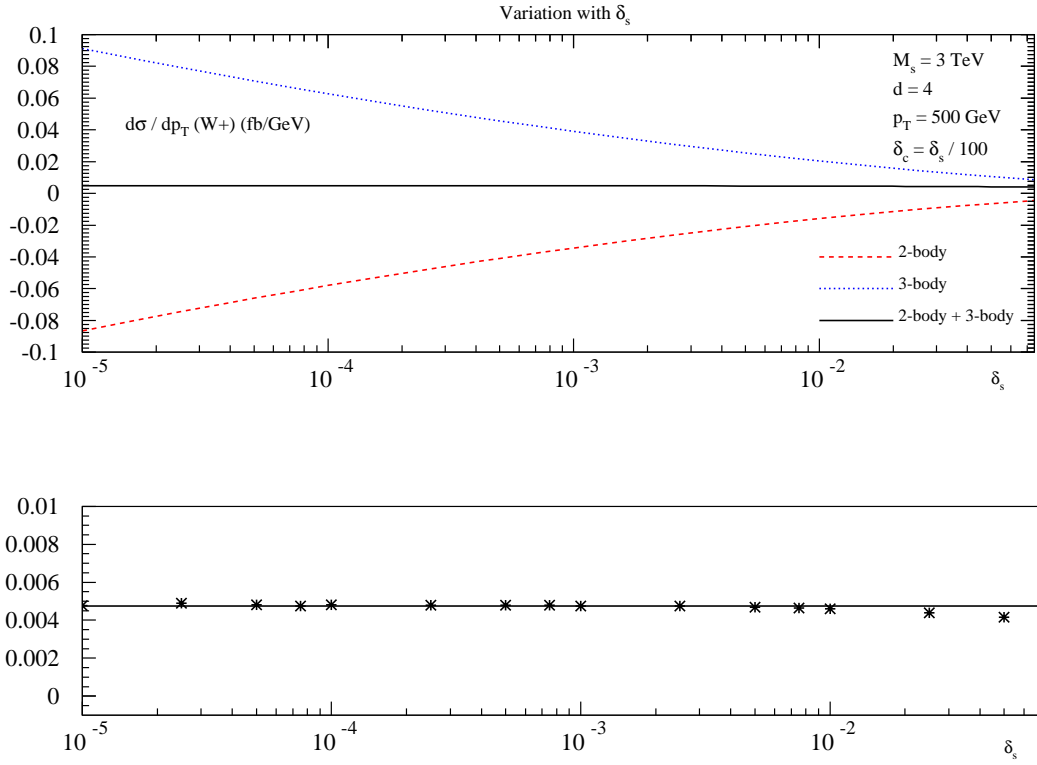


Figure 20: Variation of the transverse momentum distribution of W^+ boson with δ_s , keeping the ratio $\delta_s/\delta_c = 100$ fixed, for $M_s = 3 \text{ TeV}$ and $d = 4$.

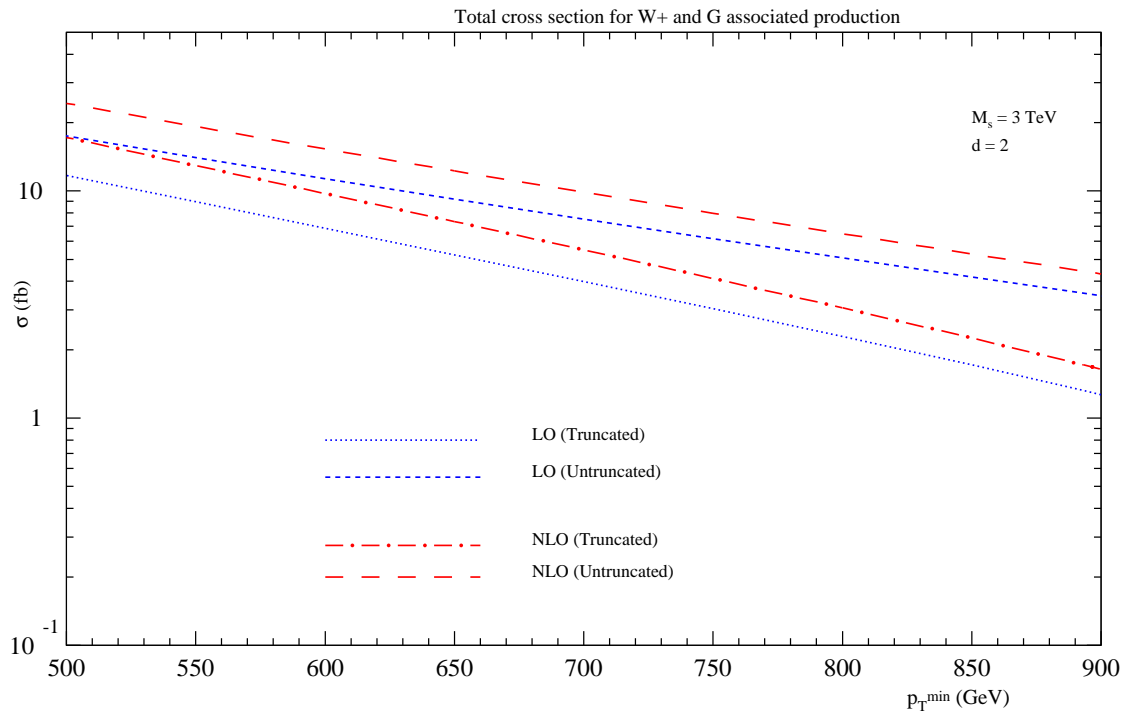


Figure 21: Total cross section for the associated production of W^+ boson and the graviton at the LHC, shown as a function of P_T^{min} for $M_s = 3 \text{ TeV}$ and $d = 2$.

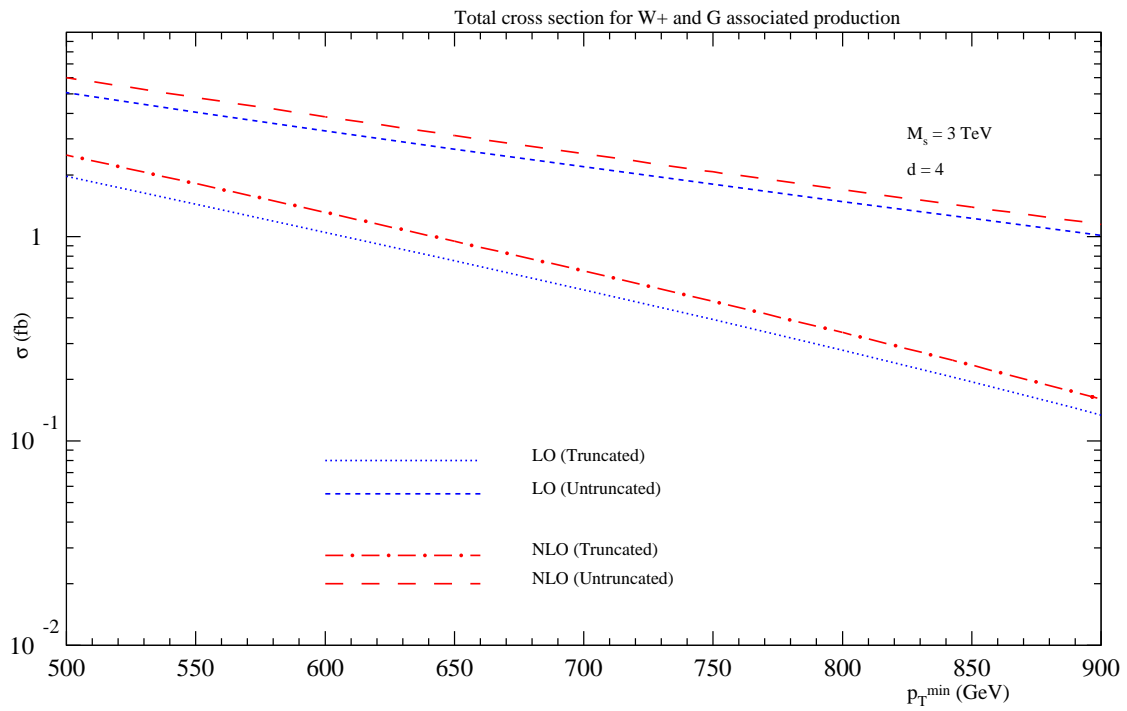


Figure 22: Total cross section for the associated production of W^+ boson and the graviton at the LHC, shown as a function of P_T^{\min} for $M_s = 3 \text{ TeV}$ and $d = 4$.

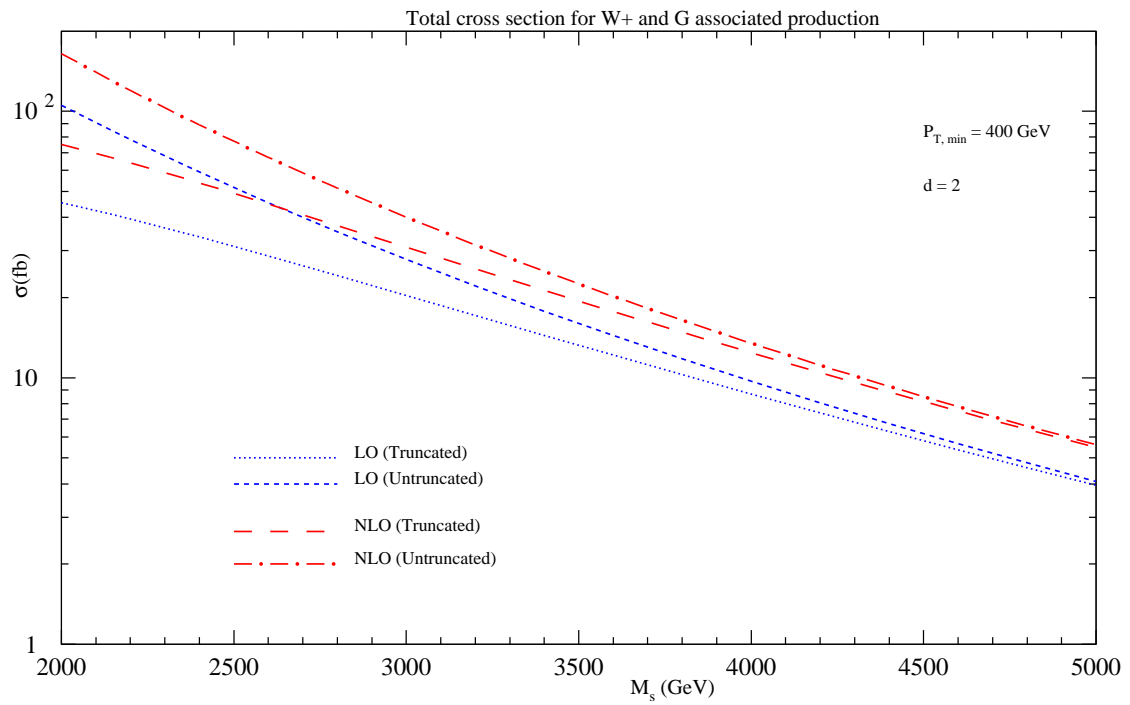


Figure 23: Total cross section for the associated production of W^+ boson and the graviton at the LHC, shown as a function of M_s for $d = 2$.

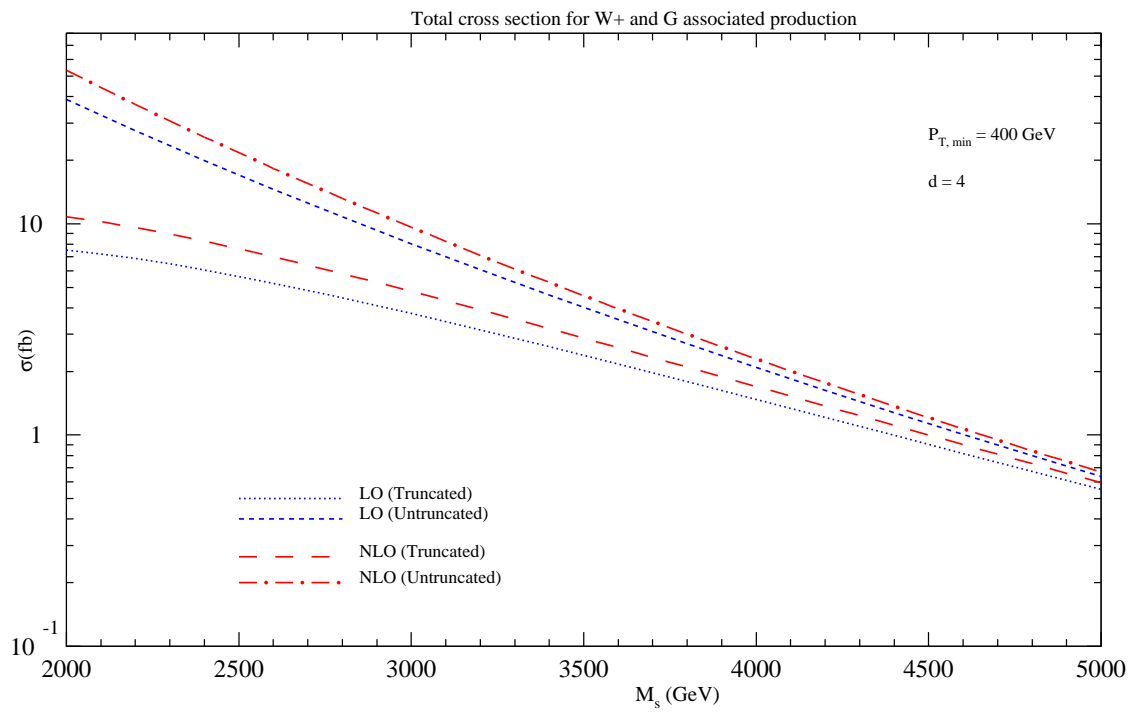


Figure 24: Total cross section for the associated production of W^+ boson and the graviton at the LHC, shown as a function of M_s for $d = 4$.

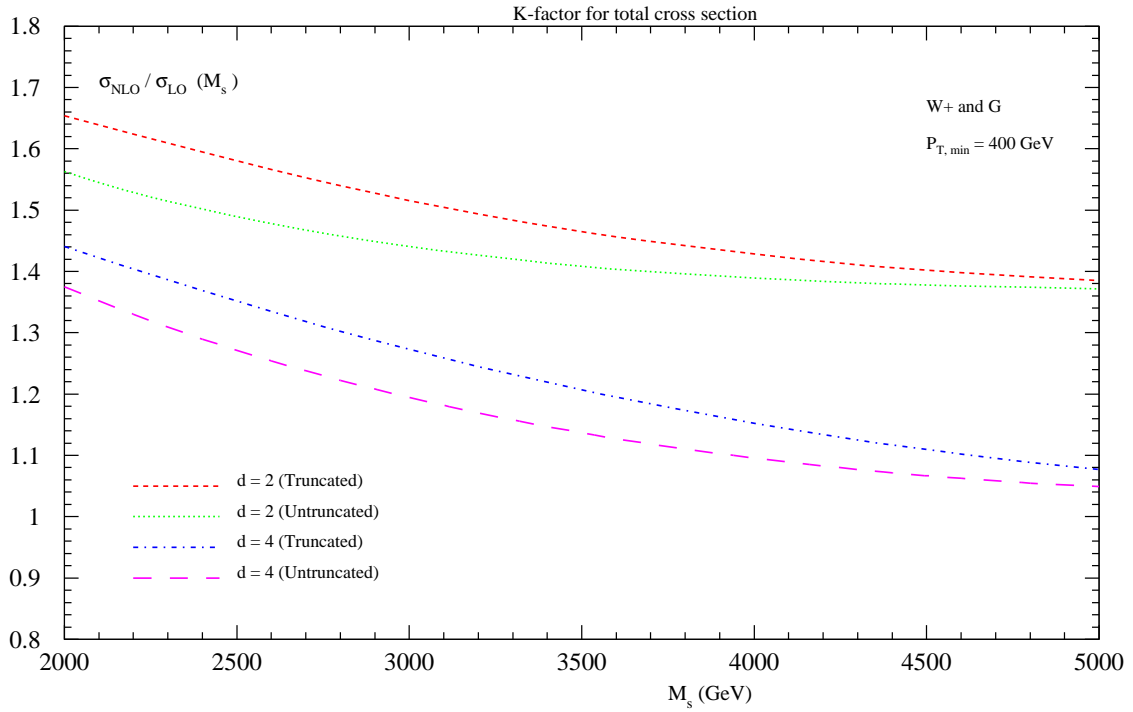
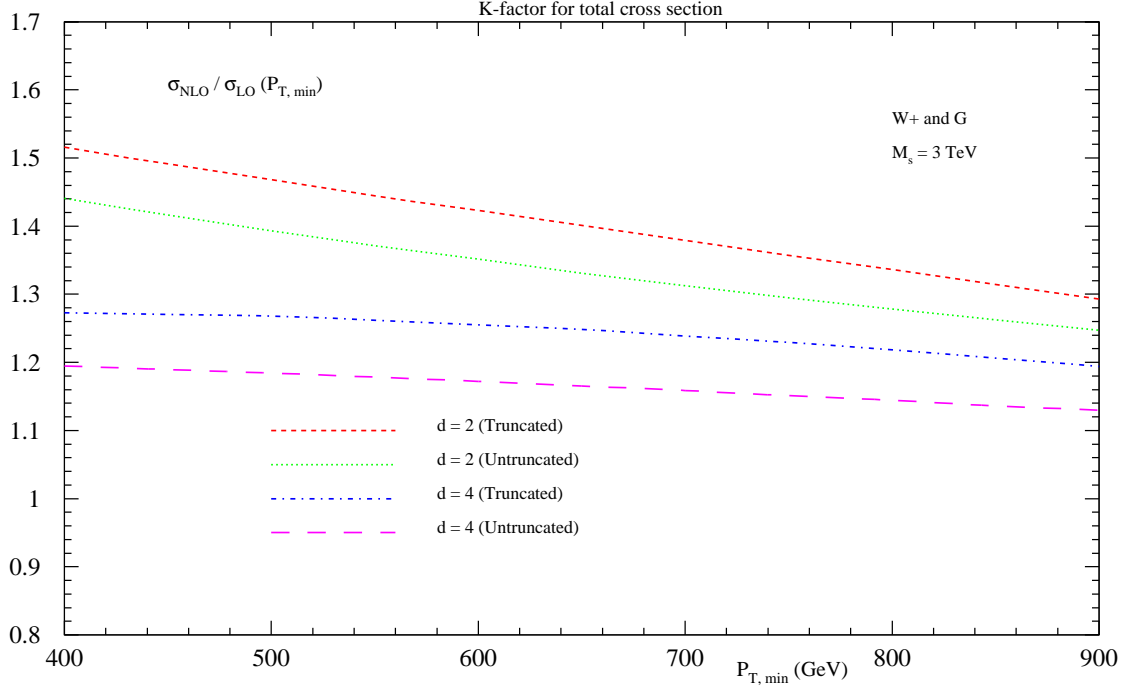


Figure 25: K-factors of the total cross section for the associated production of W^+ boson and the graviton at the LHC, given as a function of P_T^{min} (top) and the scale M_s (bottom).

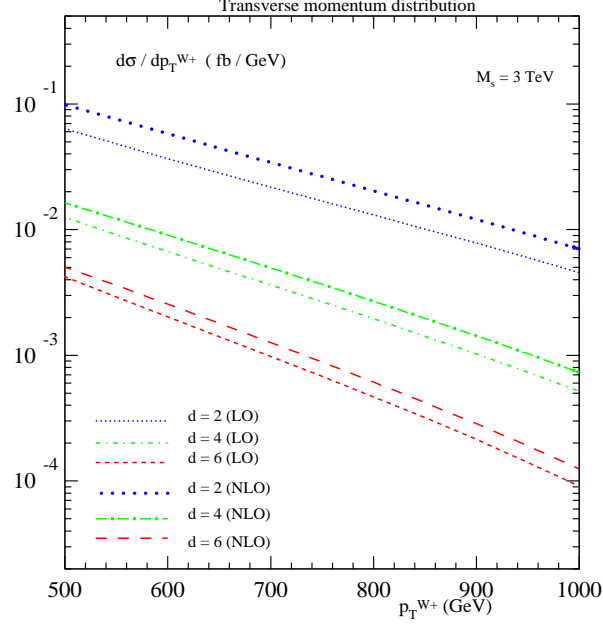


Figure 26: Transverse momentum distribution of the W^+ -boson for $M_s = 3$ TeV is shown for different values of the number of extra dimensions d .

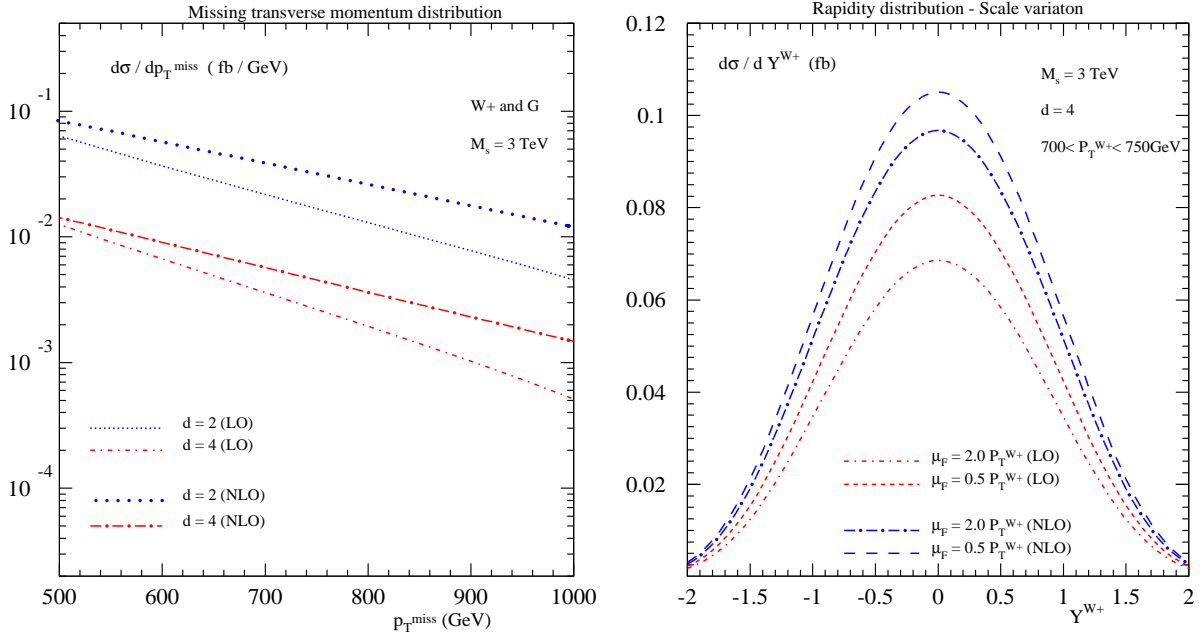


Figure 27: Missing transverse momentum distribution of the graviton produced in association with W^+ -boson at the LHC, for $M_s = 3$ TeV (left). The scale uncertainties in the rapidity distribution of W^+ -boson for $M_s = 3$ TeV and $d = 4$ (right).

References

- [1] N. Arkani-Hamed, S. Dimopoulos and G. Dvali, Phys. Lett. B 429 (1998) 263; I. Antoniadis, N. Arkani-Hamed, S. Dimopoulos and G. Dvali, Phys. Lett. B 436 (1998) 257; N. Arkani-Hamed, S. Dimopoulos and G. Dvali, Phys. Rev. D59 (1999) 086004.
- [2] D. J. Kapner et al. Phys. Rev. Lett. 98 (2007) 021101.
- [3] G. F. Giudice, R. Rattazzi, and J. D. Wells, Nucl. Phys. B544 (1999) 3.
- [4] T. Han, J. D. Lykken and R. J. Zhang, Phys. Rev. D59 (1999) 105006
- [5] P. Mathews, V. Ravindran and K. Sridhar, JHEP **0408** (2004) 048.
- [6] Prakash Mathews, V. Ravindran, K. Sridhar and W. L. van Neerven, Nucl. Phys. B713 (2005) 333; Prakash Mathews, V. Ravindran, K. Sridhar, JHEP 0510 (2005) 031; Prakash Mathews, V. Ravindran, Nucl. Phys. B753 (2006) 1; M.C. Kumar, Prakash Mathews, V. Ravindran, Eur. Phys. J. C49 (2007) 599.
- [7] E. A. Mirabelli, M. Perelstein and M. E. Peskin, Phys. Rev. Lett. 82 (1999) 2236.
- [8] Prakash Mathews, Sreerup Raychaudhuri, K. Sridhar, Phys. Lett. B450 (1999) 343; Phys. Lett. B455 (1999) 115; JHEP 0007 (2000) 008.
- [9] X. G. Wu and Z. Y. Fang, Phys. Rev. D78 (2008) 094002.
- [10] M.C. Kumar, Prakash Mathews, V. Ravindran, Anurag Tripathi, Phys. Lett. B672 (2009) 45; Nucl. Phys. B818 (2009) 28.
- [11] Neelima Agarwal, V. Ravindran, V. K. Tiwari, Anurag Tripathi, Nucl. Phys. B830 (2010) 248; Phys. Lett. B686 (2010) 244;
- [12] N. Agarwal, V. Ravindran, V. K. Tiwari and A. Tripathi, Phys. Lett. B **690** (2010) 390; Phys. Rev. D **82** (2010) 036001.
- [13] S. Karg, M. Karämer, Q. Li, D. Zeppenfeld, arXiv:0911.5095.
- [14] X Gao, C S Li, J Gao and J Wang, Phys. Rev. D81 (2010) 036008.
- [15] Kingman Cheung and Wai-Yee Keung, Phys. Rev. D60 (1999) 112003.
- [16] Gian F. Giudice, Tilman Plehn, Alessandro Strumia, Nucl. Phys. B706 (2005) 455.
- [17] Stefan Ask, Eur. Phys. J. C60 (2009) 509.

- [18] S. Ask, I.V. Akin, L. Benucci, A. De Roeck, M. Goebel, J. Haller, *Comp. Phys. Comm.* **181** (2010), 1593.
- [19] G. Aad et al. (ATLAS collaboration), CERN-OPEN-2008-020, arXiv:0901.0512v1[hep-ex].
- [20] M.C. Kumar, P. Mathews, V. Ravindran, S. Seth, arXiv:1004.5519 [hep-ph].
- [21] J. A. M. Vermaseren, math-ph/0010025.
- [22] M. Chanowitz, M. Furman and I. Hinchliffe, *Nucl. Phys.* **B159** (1979) 225.
- [23] B.W. Harris, J.F. Owens, *Phys. Rev. D* **65** (2002) 094032.
- [24] G. Duplancic and B. Nizic, *Eur. Phys. J. C* **20** (2001) 357.
- [25] K. Nakamura et. al. *Journal of Physics G* **37**, 075021 (2010).
- [26] P. M. Nadolsky *et al.*, *Phys. Rev. D* **78** (2008) 013004

Appendix A

1 Finite part of the virtual contribution

All the V_i 's appearing in eqn. (16) are given below:

$$\begin{aligned}
V_1 &= \frac{1}{(t^2 u(m_Z^2 - s))} \left((-2m^8 t + 2m^6(m_Z^2(-6t + u) + t(7t + 2u)) - m^4(18m_Z^4 t \right. \\
&\quad - 2m_Z^2(24t^2 + 6tu - u^2) + 3t(10t^2 + 8tu + u^2)) + m^2 t(-8m_Z^6 + 26t^3 + 36t^2 u \\
&\quad + 15tu^2 + u^3 + 2m_Z^4(21t + 5u) - 2m_Z^2(30t^2 + 23tu + u^2)) - 4t^2(-2m_Z^6 + 2t^3 \\
&\quad \left. + 4t^2 u + 3tu^2 + u^3 + m_Z^4(6t + 4u) - m_Z^2(6t^2 + 8tu + 3u^2)) \right) \\
V_2 &= \frac{1}{(t^2 u(m_Z^2 - s))} \left(16(2m^8 t + 2m^6(m_Z^2(6t - u) - t(7t + 2u)) + m^4(18m_Z^4 t \right. \\
&\quad - 2m_Z^2(24t^2 + 6tu - u^2) + 3t(10t^2 + 8tu + u^2)) - m^2 t(-8m_Z^6 + 26t^3 + 36t^2 u \\
&\quad + 15tu^2 + u^3 + 2m_Z^4(21t + 5u) - 2m_Z^2(30t^2 + 23tu + u^2)) + 4t^2(-2m_Z^6 + 2t^3 \\
&\quad \left. + 4t^2 u + 3tu^2 + u^3 + m_Z^4(6t + 4u) - m_Z^2(6t^2 + 8tu + 3u^2)) \right) \\
V_3 &= V_2|_{t \leftrightarrow u} \\
V_4 &= V_1|_{t \leftrightarrow u}
\end{aligned}$$

$$\begin{aligned}
V_5 = & \frac{1}{(2t^2u^2(-m^2 + t + u))}((4m^8tu - 2m^6(9tu(t + u) + m_Z^2(t^2 - 12tu + u^2)) \\
& + m^4(36m_Z^4tu + 3tu(11t^2 + 16tu + 11u^2) + 2m_Z^2(t^3 - 30t^2u - 30tu^2 + u^3)) \\
& + 4tu(-2m_Z^6(t + u) + (t + u)^2(2t^2 + tu + 2u^2) + m_Z^4(6t^2 + 8tu + 6u^2) \\
& - m_Z^2(6t^3 + 11t^2u + 11tu^2 + 6u^3)) - m^2tu(-16m_Z^6 + 52m_Z^4(t + u) \\
& - 2m_Z^2(31t^2 + 46tu + 31u^2) + 3(9t^3 + 17t^2u + 17tu^2 + 9u^3)))
\end{aligned}$$

$$\begin{aligned}
V_6 = & \frac{1}{(2t^2u^2(-m^2 + t + u))}((4m^8tu - 2m^6(9tu(t + u) + m_Z^2(t^2 - 12tu + u^2)) \\
& + m^4(36m_Z^4tu + 3tu(11t^2 + 16tu + 11u^2) + 2m_Z^2(t^3 - 30t^2u - 30tu^2 + u^3)) \\
& + 4tu(-2m_Z^6(t + u) + (t + u)^2(2t^2 + tu + 2u^2) + m_Z^4(6t^2 + 8tu + 6u^2) \\
& - m_Z^2(6t^3 + 11t^2u + 11tu^2 + 6u^3)) - m^2tu(-16m_Z^6 + 52m_Z^4(t + u) \\
& - 2m_Z^2(31t^2 + 46tu + 31u^2) + 3(9t^3 + 17t^2u + 17tu^2 + 9u^3)))
\end{aligned}$$

$$V_7 = V_6$$

$$\begin{aligned}
V_8 = & \frac{1}{((m^2 - t)^2(m_Z^2 - t)^2t^2(m^2 - t - u)u)}((m^{12}m_Z^2t(-3m_Z^2 + 2t) \\
& - 3m^{10}m_Z^2(m_Z^4(6t - u) + t^2(6t + u) - m_Z^2t(13t + u)) + m^8(-27m_Z^8t \\
& + 12t^4u + 3m_Z^6(38t^2 + 5tu - u^2) + m_Z^2t^2(48t^2 + 11tu + 3u^2) \\
& - m_Z^4t(138t^2 + 50tu + 3u^2)) - 4t^5u(4m_Z^6 - 2m_Z^4(5t + 4u) \\
& - t(2t^2 + 5tu + 3u^2) + m_Z^2(8t^2 + 13tu + 4u^2)) + m^4t^2(12m_Z^{10} \\
& - 2m_Z^8(39t + 7u) + m_Z^6(160t^2 + 61tu + 5u^2) + t^2u(56t^2 + 69tu + 12u^2) \\
& + m_Z^2t(34t^3 - 107t^2u - 99tu^2 - 12u^3) - 2m_Z^4(64t^3 + t^2u - 2tu^2 + 3u^3)) \\
& + m^6t(-12m_Z^{10} - 27m_Z^6t(8t + 3u) - 6t^3u(7t + 4u) + m_Z^8(89t + 15u) \\
& + m_Z^2t(-58t^3 + 29t^2u + 16tu^2 - 2u^3) + m_Z^4(198t^3 + 94t^2u + 23tu^2 + 3u^3)) \\
& + m^2t^3(4m_Z^8(4t - u) + 4m_Z^4t(8t^2 - 22tu - 17u^2) + 4m_Z^6(-10t^2 + 6tu + u^2) \\
& - t^2u(34t^2 + 65tu + 27u^2) + 2m_Z^2t(-4t^3 + 51t^2u + 69tu^2 + 18u^3)))
\end{aligned}$$

$$V_9 = V_8|_{t \leftrightarrow u}$$

$$\begin{aligned}
V_{10} = & -\frac{1}{(tu(-m^2 + t + u)(-4m^2m_Z^2 + (t + u)^2)^2)}(16(104m^{12}m_Z^4(t + u) \\
& + 4m^{10}m_Z^2(96m_Z^4(t + u) - 2m_Z^2(73t^2 + 74tu + 73u^2) - 3(t^3 + 13t^2u
\end{aligned}$$

$$\begin{aligned}
& +13tu^2 + u^3)) + 4(t+u)^5(-2m_Z^6(t+u) + (t+u)^2(2t^2 + tu + 2u^2) \\
& +m_Z^4(6t^2 + 8tu + 6u^2) - m_Z^2(6t^3 + 11t^2u + 11tu^2 + 6u^3)) \\
& +m^4(3(t+u)^5(11t^2 + 16tu + 11u^2) - 16m_Z^{10}(17t^2 + 10tu + 17u^2) \\
& -8m_Z^4(t+u)^3(25t^2 + 132tu + 25u^2) - 12m_Z^6(t+u)^2(43t^2 - 108tu + 43u^2) \\
& +4m_Z^2(t+u)^4(49t^2 + 40tu + 49u^2) + 48m_Z^8(16t^3 + 11t^2u + 11tu^2 + 16u^3)) \\
& -m^2(t+u)^2(-16m_Z^8(4t^2 + 11tu + 4u^2) + 2m_Z^2(t+u)^3(9t^2 - 26tu + 9u^2) \\
& +3(t+u)^4(9t^2 + 8tu + 9u^2) - 4m_Z^4(t+u)^2(45t^2 + 26tu + 45u^2) \\
& +8m_Z^6(25t^3 + 64t^2u + 64tu^2 + 25u^3)) + 4m^8(146m_Z^8(t+u) + (t+u)^5 \\
& +26m_Z^2(t+u)^2(t^2 + 5tu + u^2) - 24m_Z^6(17t^2 + 16tu + 17u^2) \\
& +4m_Z^4(69t^3 + 59t^2u + 59tu^2 + 69u^3)) + 2m^6(136m_Z^{10}(t+u) - 9(t+u)^6 \\
& -12m_Z^8(59t^2 + 54tu + 59u^2) - m_Z^2(t+u)^3(123t^2 + 286tu + 123u^2) \\
& -2m_Z^4(t+u)^2(157t^2 - 374tu + 157u^2) + m_Z^6(986t^3 + 866t^2u \\
& +866tu^2 + 986u^3))\pi^2)
\end{aligned}$$

$$\begin{aligned}
V_{11} = & -\frac{1}{(t^2u^2(-m^2 + t + u)(-4m^2m_Z^2 + (t + u)^2)^2)}((-96m^{12}m_Z^4tu \\
& -4t^2u^2(t + u)^3(-6m_Z^6 + 16m_Z^4(t + u) - 15m_Z^2(t + u)^2 + 5(t + u)^3) \\
& +4m^{10}m_Z^2(120m_Z^2tu(t + u) + tu(-3t^2 + 34tu - 3u^2) + 12m_Z^4(t^2 \\
& -12tu + u^2)) + m^2tu(2m_Z^2(t + u)^4(t^2 + 18tu + u^2) + (t + u)^5(3t^2 \\
& +64tu + 3u^2) + 2m_Z^4(t + u)^3(9t^2 - 272tu + 9u^2) - 4m_Z^6(t + u)^2(11t^2 \\
& -196tu + 11u^2) + 24m_Z^8(t^3 - 13t^2u - 13tu^2 + u^3)) + m^4(192m_Z^{10}tu(t + u) \\
& -9tu(t + u)^4(t^2 + 8tu + u^2) - 8m_Z^8tu(71t^2 + 30tu + 71u^2) \\
& -2m_Z^4tu(t + u)^2(167t^2 - 1060tu + 167u^2) + 4m_Z^6tu(167t^3 - 227t^2u \\
& -227tu^2 + 167u^3) - m_Z^2(t + u)^3(3t^4 - 20t^3u + 674t^2u^2 - 20tu^3 + 3u^4)) \\
& -2m^8(432m_Z^8tu + tu(t + u)^2(3t^2 - 4tu + 3u^2) + 2m_Z^2tu(-15t^3 + 179t^2u \\
& +179tu^2 - 15u^3) + 8m_Z^6(3t^3 - 97t^2u - 97tu^2 + 3u^3) + 4m_Z^4(3t^4 + 118t^3u \\
& +66t^2u^2 + 118tu^3 + 3u^4)) + m^6(-384m_Z^{10}tu + 1312m_Z^8tu(t + u) \\
& +4tu(t + u)^3(3t^2 + 5tu + 3u^2) - 4m_Z^6tu(391t^2 + 294tu + 391u^2)
\end{aligned}$$

$$\begin{aligned}
& +m_Z^2(t+u)^2(3t^4 - 70t^3u + 1230t^2u^2 - 70tu^3 + 3u^4) + 8m_Z^4(3t^5 + 111t^4u \\
& - 122t^3u^2 - 122t^2u^3 + 111tu^4 + 3u^5))
\end{aligned}$$

$$V_{12} = \frac{1}{(3(m^2 - t)t^2(-m_Z^2 + t)(m^2 - u)u^2(-m_Z^2 + u)(m_Z^2 - s)^2(4m^2m_Z^2 - (t + u)^2))}$$

$$\begin{aligned}
& \times ((-12m^{16}m_Z^2tu(22m_Z^4 + 20tu - 21m_Z^2(t + u)) + 3m^{14}(20t^2u^2(t + u)^2 \\
& + 44m_Z^8(t^2 - 12tu + u^2) - 10m_Z^4tu(29t^2 + 118tu + 29u^2) + m_Z^6(-44t^3 \\
& + 852t^2u + 852tu^2 - 44u^3) - 21m_Z^2tu(t^3 - 13t^2u - 13tu^2 + u^3)) \\
& + 4t^3u^3(t + u)^2(64m_Z^{10} - 176m_Z^8(t + u) + 8m_Z^6(23t^2 + 49tu + 23u^2) \\
& - 3tu(7t^3 + 5t^2u + 5tu^2 + 7u^3) - 6m_Z^4(16t^3 + 51t^2u + 51tu^2 + 16u^3) \\
& + m_Z^2(24t^4 + 111t^3u + 134t^2u^2 + 111tu^3 + 24u^4)) - 3m^{12}(792m_Z^{10}tu \\
& + 4m_Z^8(33t^3 - 601t^2u - 601tu^2 + 33u^3) + t^2u^2(79t^3 + 257t^2u + 257tu^2 \\
& + 79u^3) + m_Z^6(-121t^4 + 2026t^3u + 5262t^2u^2 + 2026tu^3 - 121u^4) \\
& + m_Z^2tu(-73t^4 + 142t^3u + 574t^2u^2 + 142tu^3 - 73u^4) - m_Z^4(11t^5 \\
& + 326t^4u + 3015t^3u^2 + 3015t^2u^3 + 326tu^4 + 11u^5)) - 3m^{10}(352m_Z^{12}tu \\
& - 2428m_Z^{10}tu(t + u) - t^2u^2(t + u)^2(127t^2 + 386tu + 127u^2) \\
& - 22m_Z^8(6t^4 - 167t^3u - 430t^2u^2 - 167tu^3 + 6u^4) + m_Z^6(99t^5 - 1796t^4u \\
& - 9887t^3u^2 - 9887t^2u^3 - 1796tu^4 + 99u^5) + m_Z^2tu(104t^5 + 521t^4u \\
& + 707t^3u^2 + 707t^2u^3 + 521tu^4 + 104u^5) + m_Z^4(33t^6 + 87t^5u + 2369t^4u^2 \\
& + 6046t^3u^3 + 2369t^2u^4 + 87tu^5 + 33u^6)) + m^8(2112m_Z^{12}tu(t + u) \\
& - 16m_Z^{10}tu(453t^2 + 1241tu + 453u^2) + m_Z^8(-132t^5 + 6321t^4u \\
& + 36839t^3u^2 + 36839t^2u^3 + 6321tu^4 - 132u^5) - 3t^2u^2(107t^5 + 809t^4u \\
& + 1912t^3u^2 + 1912t^2u^3 + 809tu^4 + 107u^5) + m_Z^6(33t^6 - 1209t^5u \\
& - 20115t^4u^2 - 42434t^3u^3 - 20115t^2u^4 - 1209tu^5 + 33u^6) + 3m_Z^2tu(84t^6 \\
& + 943t^5u + 3098t^4u^2 + 4694t^3u^3 + 3098t^2u^4 + 943tu^5 + 84u^6) + 3m_Z^4(33t^7 \\
& - 77t^6u - 544t^5u^2 + 1792t^4u^3 + 1792t^3u^4 - 544t^2u^5 - 77tu^6 + 33u^7)) \\
& + m^2t^2u^2(-1024m_Z^{12}tu - m_Z^6(t + u)^3(1033t^2 + 3430tu + 1033u^2) \\
& - 32m_Z^{10}(14t^3 - 37t^2u - 37tu^2 + 14u^3) + 3tu(t + u)^2(41t^4 + 170t^3u
\end{aligned}$$

$$\begin{aligned}
& +194t^2u^2 + 170tu^3 + 41u^4) + 8m_Z^8(142t^4 + 405t^3u + 478t^2u^2 + 405tu^3 \\
& +142u^4) + m_Z^4(483t^6 + 4326t^5u + 13853t^4u^2 + 20660t^3u^3 + 13853t^2u^4 \\
& +4326tu^5 + 483u^6) - 2m_Z^2(69t^7 + 660t^6u + 2578t^5u^2 + 5301t^4u^3 \\
& +5301t^3u^4 + 2578t^2u^5 + 660tu^6 + 69u^7) + m^6(-32m_Z^{12}tu(33t^2 \\
& +131tu + 33u^2) + 4m_Z^{10}tu(537t^3 + 4225t^2u + 4225tu^2 + 537u^3) \\
& +3t^2u^2(t+u)^2(49t^4 + 469t^3u + 862t^2u^2 + 469tu^3 + 49u^4) - 4m_Z^8tu(126t^4 \\
& +4141t^3u + 9014t^2u^2 + 4141tu^3 + 126u^4) + m_Z^6(33t^7 - 630t^6u + 775t^5u^2 \\
& +14222t^4u^3 + 14222t^3u^4 + 775t^2u^5 - 630tu^6 + 33u^7) - 3m_Z^2tu(43t^7 \\
& +686t^6u + 3478t^5u^2 + 7861t^4u^3 + 7861t^3u^4 + 3478t^2u^5 + 686tu^6 + 43u^7) \\
& +m_Z^4(-33t^8 + 171t^7u + 5013t^6u^2 + 15053t^5u^3 + 18824t^4u^4 + 15053t^3u^5 \\
& +5013t^2u^6 + 171tu^7 - 33u^8)) + m^4tu(2080m_Z^{12}tu(t+u) \\
& -6tu(t+u)^3(5t^4 + 96t^3u + 172t^2u^2 + 96tu^3 + 5u^4) + 8m_Z^{10}(24t^4 \\
& -485t^3u - 1382t^2u^2 - 485tu^3 + 24u^4) - m_Z^8(423t^5 + 375t^4u - 8054t^3u^2 \\
& -8054t^2u^3 + 375tu^4 + 423u^5) + m_Z^6(237t^6 + 3942t^5u + 10563t^4u^2 \\
& +11668t^3u^3 + 10563t^2u^4 + 3942tu^5 + 237u^6) - m_Z^4(39t^7 + 2514t^6u \\
& +14408t^5u^2 + 29959t^4u^3 + 29959t^3u^4 + 14408t^2u^5 + 2514tu^6 + 39u^7) \\
& +m_Z^2(33t^8 + 777t^7u + 5388t^6u^2 + 16631t^5u^3 + 24742t^4u^4 + 16631t^3u^5 \\
& +5388t^2u^6 + 777tu^7 + 33u^8))))
\end{aligned}$$

$$\begin{aligned}
V_{13} = & \frac{1}{((m_Z^2 - t)^2 t^2 (m_Z^2 - u)^2 u^2 (-m^2 + t + u) (-4m^2 m_Z^2 + (t + u)^2)^2)} \\
& \times (m_Z^2 (-16m^{12} m_Z^4 tu (6m_Z^6 - 8m_Z^4 (t + u) - 2tu(t + u) + m_Z^2 (3t^2 + 8tu \\
& + 3u^2)) + 8m^{10} m_Z^2 (6m_Z^{10} (t^2 - 12tu + u^2) + m_Z^8 (-12t^3 + 149t^2u + 149tu^2 \\
& - 12u^3) + 3m_Z^4 tu (t^3 + 45t^2u + 45tu^2 + u^3) - t^2u^2 (2t^3 + t^2u + tu^2 + 2u^3) \\
& + m_Z^2 tu (3t^4 - 2t^3u - 54t^2u^2 - 2tu^3 + 3u^4) + m_Z^6 (6t^4 - 80t^3u - 284t^2u^2 \\
& - 80tu^3 + 6u^4)) + 4t^2u^2 (t + u)^3 (6m_Z^{12} - 28m_Z^{10} (t + u) + 2tu(t + u)^2 (t^2 \\
& + 3tu + u^2) + m_Z^8 (49t^2 + 110tu + 49u^2) - m_Z^6 (41t^3 + 155t^2u + 155tu^2 \\
& + 41u^3) + m_Z^4 (17t^4 + 97t^3u + 166t^2u^2 + 97tu^3 + 17u^4) - m_Z^2 (3t^5 + 26t^4u
\end{aligned}$$

$$\begin{aligned}
& +71t^3u^2 + 71t^2u^3 + 26tu^4 + 3u^5)) - m^8(864m_Z^{14}tu + 24m_Z^{12}(2t^3 - 117t^2u \\
& - 117tu^2 + 2u^3) - 4m_Z^8tu(293t^3 + 1581t^2u + 1581tu^2 + 293u^3) \\
& + m_Z^{10}(-72t^4 + 3012t^3u + 7672t^2u^2 + 3012tu^3 - 72u^4) - 2t^2u^2(t^5 + 15t^4u \\
& - 20t^3u^2 - 20t^2u^3 + 15tu^4 + u^5) - 4m_Z^4tu(t^5 + 19t^4u - 54t^3u^2 \\
& - 54t^2u^3 + 19tu^4 + u^5) + m_Z^2tu(3t^6 + 36t^5u - 23t^4u^2 - 688t^3u^3 \\
& - 23t^2u^4 + 36tu^5 + 3u^6) + 2m_Z^6(12t^6 + 57t^5u + 812t^4u^2 + 1470t^3u^3 \\
& + 812t^2u^4 + 57tu^5 + 12u^6)) - m^2tu(4m_Z^{12}(t + u)^2(23t^2 - 352tu + 23u^2) \\
& - 24m_Z^{14}(t^3 - 13t^2u - 13tu^2 + u^3) + 2tu(t + u)^4(t^4 + 13t^3u + 38t^2u^2 \\
& + 13tu^3 + u^4) + 2m_Z^8(t + u)^2(59t^4 - 542t^3u - 2218t^2u^2 - 542tu^3 + 59u^4) \\
& - 2m_Z^{10}(73t^5 - 845t^4u - 3284t^3u^2 - 3284t^2u^3 - 845tu^4 + 73u^5) \\
& - m_Z^2(t + u)^3(3t^6 + 48t^5u + 237t^4u^2 + 236t^3u^3 + 237t^2u^4 + 48tu^5 + 3u^6) \\
& + 2m_Z^4(t + u)^2(6t^6 + 87t^5u + 104t^4u^2 - 238t^3u^3 + 104t^2u^4 + 87tu^5 + 6u^6) \\
& + m_Z^6(-49t^7 - 73t^6u + 2017t^5u^2 + 6457t^4u^3 + 6457t^3u^4 + 2017t^2u^5 \\
& - 73tu^6 - 49u^7)) + m^6(-384m_Z^{16}tu + 1936m_Z^{14}tu(t + u) - 4m_Z^{12}tu(859t^2 \\
& + 1806tu + 859u^2) - t^2u^2(t + u)^2(3t^4 + 64t^3u - 130t^2u^2 + 64tu^3 + 3u^4) \\
& + 8m_Z^{10}(3t^5 + 347t^4u + 1095t^3u^2 + 1095t^2u^3 + 347tu^4 + 3u^5) - m_Z^8(45t^6 \\
& + 1146t^5u + 3887t^4u^2 + 3460t^3u^3 + 3887t^2u^4 + 1146tu^5 + 45u^6) + m_Z^2tu(3t^7 \\
& + 115t^6u + 165t^5u^2 - 1811t^4u^3 - 1811t^3u^4 + 165t^2u^5 + 115tu^6 + 3u^7) \\
& + 2m_Z^6(9t^7 + 142t^6u + 348t^5u^2 - 1971t^4u^3 - 1971t^3u^4 + 348t^2u^5 + 142tu^6 \\
& + 9u^7) + m_Z^4(3t^8 - 32t^7u - 340t^6u^2 + 2156t^5u^3 + 6490t^4u^4 + 2156t^3u^5 \\
& - 340t^2u^6 - 32tu^7 + 3u^8)) + m^4(192m_Z^{16}tu(t + u) - 8m_Z^{14}tu(101t^2 \\
& + 138tu + 101u^2) + 4m_Z^{12}tu(333t^3 + 379t^2u + 379tu^2 + 333u^3) \\
& + 2m_Z^{10}tu(-581t^4 + 30t^3u + 2118t^2u^2 + 30tu^3 - 581u^4) + 3t^2u^2(t + u)^3(t^4 \\
& + 18t^3u - 2t^2u^2 + 18tu^3 + u^4) - m_Z^2tu(t + u)^2(3t^6 + 96t^5u + 209t^4u^2 \\
& - 1132t^3u^3 + 209t^2u^4 + 96tu^5 + 3u^6) - m_Z^8(3t^7 - 613t^6u + 921t^5u^2 \\
& + 11961t^4u^3 + 11961t^3u^4 + 921t^2u^5 - 613tu^6 + 3u^7) + m_Z^6(6t^8 - 177t^7u
\end{aligned}$$

$$\begin{aligned}
& +12t^6u^2 + 8745t^5u^3 + 18124t^4u^4 + 8745t^3u^5 + 12t^2u^6 - 177tu^7 + 6u^8) \\
& -m_Z^4(3t^9 - 13t^8u - 338t^7u^2 + 1474t^6u^3 + 8410t^5u^4 + 8410t^4u^5 \\
& +1474t^3u^6 - 338t^2u^7 - 13tu^8 + 3u^9))) \\
V_{14} = & \frac{1}{((m^2 - t)^2t^2(m^2 - u)^2(m^2 - t - u)u^2(-4m^2m_Z^2 + (t + u)^2)^2)} \\
& (m^2(96m^{18}m_Z^4tu - 4m^{16}m_Z^2(158m_Z^2tu(t + u) + tu(-3t^2 + 34tu - 3u^2) \\
& +12m_Z^4(t^2 - 12tu + u^2)) - 4t^3u^3(t + u)^2(12m_Z^6tu + 6tu(t + u)^3 \\
& +m_Z^2(t + u)^2(t^2 - 11tu + u^2) - m_Z^4(t^3 + 7t^2u + 7tu^2 + u^3)) \\
& +2m^{14}(432m_Z^8tu + tu(t + u)^2(3t^2 - 4tu + 3u^2) - 4m_Z^2tu(8t^3 - 113t^2u \\
& -113tu^2 + 8u^3) + 4m_Z^6(18t^3 - 281t^2u - 281tu^2 + 18u^3) + 2m_Z^4(6t^4 \\
& +411t^3u + 578t^2u^2 + 411tu^3 + 6u^4)) + m^2t^2u^2(48m_Z^8tu(3t^2 - 2tu + 3u^2) \\
& +2(t + u)^4(3t^4 + 29t^3u + 72t^2u^2 + 29tu^3 + 3u^4) - m_Z^2(t + u)^3(5t^4 \\
& +124t^3u - 102t^2u^2 + 124tu^3 + 5u^4) + 2m_Z^4(t + u)^2(7t^4 + 86t^3u - 522t^2u^2 \\
& +86tu^3 + 7u^4) - 4m_Z^6(3t^5 + 61t^4u - 164t^3u^2 - 164t^2u^3 + 61tu^4 + 3u^5)) \\
& +m^{12}(384m_Z^{10}tu - 2288m_Z^8tu(t + u) - 4tu(t + u)^3(6t^2 + tu + 6u^2) - \\
& 16m_Z^6(9t^4 - 207t^3u - 416t^2u^2 - 207tu^3 + 9u^4) - 8m_Z^4(9t^5 + 284t^4u \\
& +356t^3u^2 + 356t^2u^3 + 284tu^4 + 9u^5) - m_Z^2(3t^6 - 126t^5u + 2089t^4u^2 \\
& +4756t^3u^3 + 2089t^2u^4 - 126tu^5 + 3u^6)) + m^{10}(-576m_Z^{10}tu(t + u) \\
& +672m_Z^8tu(3t^2 + 7tu + 3u^2) + tu(t + u)^2(39t^4 + 170t^3u + 222t^2u^2 \\
& +170tu^3 + 39u^4) + 16m_Z^6(3t^5 - 147t^4u - 424t^3u^2 - 424t^2u^3 - 147tu^4 \\
& +3u^5) + 2m_Z^4(36t^6 + 915t^5u + 780t^4u^2 - 1286t^3u^3 + 780t^2u^4 + 915tu^5 \\
& +36u^6) + m_Z^2(9t^7 - 109t^6u + 2141t^5u^2 + 8903t^4u^3 + 8903t^3u^4 + 2141t^2u^5 \\
& -109tu^6 + 9u^7)) - m^4tu(48m_Z^8tu(4t^3 + 3t^2u + 3tu^2 + 4u^3) \\
& -m_Z^2tu(t + u)^2(85t^4 - 52t^3u - 1286t^2u^2 - 52tu^3 + 85u^4) + (t + u)^3(3t^6 \\
& +58t^5u + 303t^4u^2 + 492t^3u^3 + 303t^2u^4 + 58tu^5 + 3u^6) - 4m_Z^6(3t^6 \\
& +108t^5u - 55t^4u^2 - 608t^3u^3 - 55t^2u^4 + 108tu^5 + 3u^6) + m_Z^4(15t^7 \\
& +353t^6u - 501t^5u^2 - 5475t^4u^3 - 5475t^3u^4 - 501t^2u^5 + 353tu^6 + 15u^7))
\end{aligned}$$

$$\begin{aligned}
& +m^8(192m_Z^{10}tu(t^2 + 4tu + u^2) - 32m_Z^8tu(20t^3 + 97t^2u + 97tu^2 + 20u^3) \\
& -3tu(t+u)^3(11t^4 + 80t^3u + 122t^2u^2 + 80tu^3 + 11u^4) + 32m_Z^6tu(27t^4 \\
& +104t^3u + 77t^2u^2 + 104tu^3 + 27u^4) - 2m_Z^4(12t^7 + 423t^6u + 483t^5u^2 \\
& -3970t^4u^3 - 3970t^3u^4 + 483t^2u^5 + 423tu^6 + 12u^7) - m_Z^2(9t^8 - 36t^7u \\
& +880t^6u^2 + 7376t^5u^3 + 13062t^4u^4 + 7376t^3u^5 + 880t^2u^6 - 36tu^7 + 9u^8)) \\
& +m^6(-192m_Z^{10}t^2u^2(t+u) + 16m_Z^8tu(3t^4 + 58t^3u + 62t^2u^2 + 58tu^3 \\
& +3u^4) - 4m_Z^6tu(41t^5 + 337t^4u - 308t^3u^2 - 308t^2u^3 + 337tu^4 + 41u^5) \\
& +tu(t+u)^2(15t^6 + 194t^5u + 697t^4u^2 + 1016t^3u^3 + 697t^2u^4 + 194tu^5 \\
& +15u^6) + m_Z^4tu(195t^6 + 916t^5u - 4815t^4u^2 - 12032t^3u^3 - 4815t^2u^4 \\
& +916tu^5 + 195u^6) + m_Z^2(3t^9 - t^8u - 20t^7u^2 + 2332t^6u^3 + 7838t^5u^4 \\
& +7838t^4u^5 + 2332t^3u^6 - 20t^2u^7 - tu^8 + 3u^9))) \\
V_{15} = & \frac{1}{(6t^2u^2(-m^2 + t + u)^2)}((144m^{10}tu - 6m^8(97tu(t+u) + 12m_Z^2(t^2 - 12tu \\
& +u^2)) + 3m^6(432m_Z^4tu + tu(353t^2 + 700tu + 353u^2) + m_Z^2(48t^3 - 746t^2u \\
& -746tu^2 + 48u^3)) + 12m^4(48m_Z^6tu - 208m_Z^4tu(t+u) - tu(89t^3 + 249t^2u \\
& +249tu^2 + 89u^3) + m_Z^2(-6t^4 + 199t^3u + 482t^2u^2 + 199tu^3 - 6u^4)) \\
& +m^2tu(-696m_Z^6(t+u) + 40m_Z^4(39t^2 + 107tu + 39u^2) - 6m_Z^2(229t^3 \\
& +817t^2u + 817tu^2 + 229u^3) + 21(27t^4 + 98t^3u + 126t^2u^2 + 98tu^3 + 27u^4)) \\
& -4tu(-2m_Z^6(15t^2 + 86tu + 15u^2) + m_Z^4(90t^3 + 406t^2u + 406tu^2 + 90u^3) \\
& -m_Z^2(90t^4 + 381t^3u + 512t^2u^2 + 381tu^3 + 90u^4) + 3(10t^5 + 49t^4u + 69t^3u^2 \\
& +69t^2u^3 + 49tu^4 + 10u^5)))) \tag{1}
\end{aligned}$$

2 B_0 Integrals

$$B_0(\mathcal{P}) = \frac{i}{(4\pi)^2} \left[-\frac{2}{\epsilon} + 2 - \gamma_E - f(\mathcal{P}) \right] \tag{2}$$

where $\mathcal{P} \in \{p_3, p_4, p_5, k, q\}$, k is the momentum of vector boson, q , the momentum of graviton, $p_3 = p_1 + k, p_4 = p_2 + k, p_5 = p_1 + p_2$ and,

$$f(\mathcal{P}) = \begin{cases} \ln\left(\frac{-\mathcal{P}^2}{4\pi\mu_r^2}\right) & \text{for } \mathcal{P} = p_3, p_4 \\ \ln\left(\frac{\mathcal{P}^2}{4\pi\mu_r^2}\right) - i\pi & \text{for } \mathcal{P} = p_5, k, q \end{cases} \quad (3)$$

3 C_0 Integrals

$$C_0(\mathcal{P}', \mathcal{P}'') = \frac{-i}{(4\pi)^2} \frac{1}{[(\mathcal{P}' - \mathcal{P}'')^2 - \mathcal{P}''^2]} \left[-\frac{2}{\epsilon} \left\{ \ln\left(\frac{-(\mathcal{P}' - \mathcal{P}'')^2}{\mathcal{P}''^2}\right) + i\pi \right\} + \frac{1}{2} \left\{ \left(\gamma_E + \ln\left(\frac{\mathcal{P}''^2}{4\pi\mu_r^2}\right) - i\pi \right)^2 - \left(\gamma_E + \ln\left(\frac{-(\mathcal{P}' - \mathcal{P}'')^2}{4\pi\mu_r^2}\right) \right)^2 \right\} \right] \quad (4)$$

where $\mathcal{P}' \in \{p_1, p_2\}$ and, $\mathcal{P}'' \in \{k, q\}$

$$C_0(p_1, p_2) = \frac{-i}{(4\pi)^2} \frac{1}{s} \left[-\frac{4}{\epsilon^2} - \frac{2}{\epsilon} \left\{ \gamma_E + \ln\left(\frac{s}{4\pi\mu_r^2}\right) - i\pi \right\} + \frac{1}{2} \left\{ \frac{\pi^2}{6} - \left(\gamma_E + \ln\left(\frac{s}{4\pi\mu_r^2}\right) - i\pi \right)^2 \right\} \right] \quad (5)$$

$$C_0(k, q) = \frac{-i}{(4\pi)^2} \frac{1}{s\beta} \left[2Li_2\left(\frac{2}{1-\alpha+\beta}\right) - 2Li_2\left(\frac{2}{1-\alpha-\beta}\right) - \ln\left(\frac{(1-\alpha)^2 - \beta^2}{4}\right) \left\{ \ln\left(\frac{\alpha-\beta+1}{\alpha-\beta-1}\right) - \ln\left(\frac{\alpha+\beta+1}{\alpha+\beta-1}\right) \right\} \right] \quad (6)$$

where $\alpha = \frac{m^2 - m_z^2}{s}$ and $\beta = \frac{1}{s} \sqrt{(t+u)^2 - 4m_z^2 m^2}$

4 D_0 Integrals

$$D_0(p_1, k, q) = \frac{i}{(4\pi)^2} \frac{1}{st} \left[\frac{4}{\epsilon^2} + \frac{2}{\epsilon} \left\{ \gamma_E + \ln\left(\frac{-t}{4\pi\mu_r^2}\right) + \ln\left(\frac{s}{m_z^2}\right) + \ln\left(\frac{-t}{m^2}\right) + i\pi \right\} + \left(\gamma_E + \ln\left(\frac{s}{4\pi\mu_r^2}\right) - i\pi \right)^2 + \left(\gamma_E + \ln\left(\frac{-t}{4\pi\mu_r^2}\right) \right)^2 - \left(\gamma_E + \ln\left(\frac{m_z^2}{4\pi\mu_r^2}\right) - i\pi \right)^2 - \left(\gamma_E + \ln\left(\frac{m^2}{4\pi\mu_r^2}\right) - i\pi \right)^2 + \frac{1}{2} \left(\gamma_E + \ln\left(\frac{m_z^2}{s}\right) + \ln\left(\frac{m^2}{4\pi\mu_r^2}\right) - i\pi \right)^2 - \frac{\pi^2}{12} \right]$$

$$\begin{aligned}
& + \frac{1}{3} \left(-3 \ln^2 \left(1 - \frac{t}{m^2} \right) - 3 \ln^2 \left(\frac{m_z^2 - t}{s} \right) - \pi^2 \right) - 2Li_2 \left(\frac{t}{m^2} \right) \\
& + \ln^2 \left(1 - \frac{m^2}{t} \right) - 2i\pi \ln \left(1 - \frac{m^2}{t} \right) - 2Li_2 \left(\frac{t}{m_z^2} \right) \\
& + 2 \ln \left(1 - \frac{m_z^2}{s} \right) \left(\ln \left(1 - \frac{m_z^2}{t} \right) - i\pi \right) \\
& + \left(\ln \left(1 - \frac{m_z^2}{t} \right) - \ln \left(\frac{m_z^2 - s}{t} \right) \right) \times \\
& \quad \left(\ln \left(\frac{m_z^2 - s}{t} \right) + \log \left(1 - \frac{m_z^2}{t} \right) - 2i\pi \right) \\
& - 2 \ln \left(\frac{s}{m_z^2} - 1 \right) \ln \left(1 - \frac{t}{m_z^2} \right) + \ln^2 \left(1 - \frac{m_z^2}{s} \right) \\
& - \ln^2 \left(\frac{s}{m_z^2} \right) + 2 \ln \left(\frac{s}{m_z^2} \right) \ln \left(\frac{s}{m_z^2} - 1 \right) \Big] \tag{7}
\end{aligned}$$

$D_0(p_2, k, q)$ can be readily obtained by replacing ‘ t ’ by ‘ u ’ in the above $D_0(p_1, k, q)$ expression.

$$\begin{aligned}
D_0(k, p_2, q) = & \frac{i}{(4\pi)^2} \frac{1}{(tu - m_z^2 m^2)} \left[\frac{4}{\epsilon} \left\{ \ln \left(\frac{-t}{m_z^2} \right) + \ln \left(\frac{-u}{m^2} \right) + 2i\pi \right\} \right. \\
& - \left(\gamma_E + \ln \left(\frac{m_z^2}{4\pi\mu_r^2} \right) - i\pi \right)^2 - \left(\gamma_E + \ln \left(\frac{m^2}{4\pi\mu_r^2} \right) - i\pi \right)^2 \\
& + \left(\gamma_E + \ln \left(\frac{-t}{4\pi\mu_r^2} \right) \right)^2 + \left(\gamma_E + \ln \left(\frac{-u}{4\pi\mu_r^2} \right) \right)^2 - \frac{4\pi^2}{3} \\
& + 2Li_2 \left(\frac{(m^2 - t)(m_z^2 - t)}{m^2 m_z^2 - tu} \right) + 2Li_2 \left(\frac{(m^2 - u)(m_z^2 - u)}{m^2 m_z^2 - tu} \right) \\
& + 2Li_2 \left(\frac{tu - m^2 m_z^2}{(m^2 - t)(m^2 - u)} \right) + 2Li_2 \left(\frac{tu - m^2 m_z^2}{(m_z^2 - t)(m_z^2 - u)} \right) \\
& + \ln^2 \left(\frac{(m^2 - t)(m^2 - u)}{tu - m^2 m_z^2} \right) + \ln^2 \left(\frac{(m_z^2 - t)(m_z^2 - u)}{tu - m^2 m_z^2} \right) \\
& \left. - 2i\pi \left(\ln \left(\frac{(m^2 - t)(m^2 - u)}{tu - m^2 m_z^2} \right) + \ln \left(\frac{(m_z^2 - t)(m_z^2 - u)}{tu - m^2 m_z^2} \right) \right) \right] \tag{8}
\end{aligned}$$

Transverse momentum distribution

